ELSEVIER

Contents lists available at ScienceDirect

Remote Sensing of Environment

journal homepage: www.elsevier.com/locate/rse



Using SMAP Level-4 soil moisture to constrain MOD16 evapotranspiration over the contiguous USA



Colin Brust ^{a,*}, John S. Kimball ^a, Marco P. Maneta ^b, Kelsey Jencso ^c, Mingzhu He ^d, Rolf H. Reichle ^e

- a Numerical Terradynamic Simulation Group, W.A. Franke College of Forestry & Conservation, University of Montana, Missoula, MT 59812, USA
- ^b Department of Geosciences, University of Montana, Missoula, MT 59812, USA
- ^c Montana Climate Office, W.A. Franke College of Forestry & Conservation, University of Montana, Missoula, MT 59812, USA
- d Sino-French Institute for Earth System Science, College of Urban and Environmental Sciences, Peking University, Beijing, 10087, China
- ^e Global Modeling and Assimilation Office, NASA Goddard Space Flight Center, 8800 Greenbelt Rd, Greenbelt, MD 20771, USA

ARTICLE INFO

Keywords: Evapotranspiration SMAP MODIS MOD16 Soil moisture

ABSTRACT

Evapotranspiration (ET) is a key hydrologic variable linking the Earth's water, carbon and energy cycles. At large spatial scales, remote sensing-based (RS) models are often used to quantify ET. Despite the large number of RS ET models available, few include soil moisture as a key environmental input, which can degrade model accuracy and utility. Here, we use model assimilation enhanced soil moisture estimates from the NASA SMAP (Soil Moisture Active Passive) mission as a water supply control in the MOD16 ET algorithm framework. SMAP-derived daily surface (0-5 cm depth) and root zone (0-1 m depth) soil moisture are used with MODIS (Moderate Resolution Imaging Spectroradiometer) vegetation observations, and 4 km gridded regional surface meteorology (Gridmet) as primary inputs for estimating daily ET and underlying model soil and stomatal conductance terms. We calibrated the model environmental response parameters using tower eddy covariance ET observations representing major North American biomes. The model ET results were validated using a holdout set of tower observations spanning a large regional climate gradient. The updated ET estimates outperform the baseline MOD16 product across all tower validation sites (RMSE = 0.758 vs 1.108 mm day⁻¹; $R^2 = 0.68$ vs 0.45, respectively). Smaller relative improvements were obtained using a recalibrated model with 4 km Gridmet meteorology, but no soil moisture control (RMSE = 0.813 mm day⁻¹; R² = 0.66), indicating that these changes are essential for the improved model performance. The soil moisture-constrained model improvements and relative benefits from the SMAP observations are greater in arid climates, consistent with stronger soil moisture control on ET in waterlimited regions. The use of SMAP soil moisture as an additional model constraint improves MOD16 regional performance and provides a new framework for investigating both soil and atmosphere controls on ET.

1. Introduction

Terrestrial evapotranspiration (ET) is the sum of transpiration through plant stomata, evaporation from the soil surface, and

evaporation from the wet plant canopy. ET is an important driver of global climate as it links the carbon, water and energy cycles via the movement of water vapor and CO₂ through plant stomata (Jung et al., 2011; Mu et al., 2007; Zhang et al., 2019a). Additionally, ET is the

Acronyms: ANOVA, Analysis of variance; BPLUT, Biome Property Look-up Table; BRO, Broadleaf croplands; CER, Cereal croplands; CONUS, Continental United States; CSH, Closed shrublands; CRO, Croplands; DBF, Deciduous broadleaf forest; DNF, Deciduous needleleaf forest; EBF, Evergreen broadleaf forest; ENF, Evergreen needleleaf forest; ET, Evapotranspiration; ET_{L4R}, ET model that uses SMAP L4_SM soil moisture and regional Gridmet meteorology; ET_{NRR}, ET model that uses Nature Run soil moisture and regional Gridmet meteorology; FPAR, Fraction of Photosynthetically Active Radiation; GEOS FP-IT, Goddard Earth Observing System Forward Processing for Instrument Teams; GRA, Grasslands; LAI, Leaf Area Index; L4_SM, SMAP Level 4 soil moisture product; OSH, Open shrublands; MF, Mixed forest; MODIS, Moderate Resolution Imaging Spectroradiometer; MOD16, Operational MOD16A2 ET product; PFT, Plant functional type; PT-JPL, Priestly-Taylor Jet Propulsion Laboratory ET model; REW, Relative extractable water; RMSE, Root mean squared error; RS, Remote sensing; SAV, Savanna; SMAP, Soil Moisture Active Passive Satellite; VPD, Vapor pressure deficit; WSA, Woody savanna.

* Corresponding author.

E-mail address: colin.brust@umontana.edu (C. Brust).

largest terrestrial water flux, returning 60–70% of the precipitation that falls on the Earth's land surface back to the atmosphere annually (Oki and Kanae, 2006; Zhang et al., 2016b). Due to its large role in the Earth's water, carbon and energy fluxes, ET is an integral component of hydrologic and land surface models that inform policy decisions (IPCC, 2014; Koster et al., 2000; Maneta and Silverman, 2013). Finer scale ET estimates are also important for evaluating water use and crop stress over complex agricultural landscapes (Allen et al., 2007; He et al., 2019a; Wurster et al., 2020). It is therefore essential that methods for estimating ET are accurate and available with suitable resolution and extent to capture characteristic ET heterogeneity.

At small spatial scales, the eddy covariance method can be used to calculate ET as a function of surface-atmosphere latent energy fluxes measured at flux towers (Baldocchi, 2003). However, flux towers only represent a limited sampling footprint, ranging from a few dozen meters (Arriga et al., 2017) to approximately 1 km in resolution (Barcza et al., 2009). Additionally, the sparse global tower network is insufficient to capture global climate and land cover diversity (Pastorello et al., 2017). A common method for augmenting and extrapolating these sparse observations is to use remote sensing-based (RS) ET models. RS ET models use satellite observations to provide temporally regular and spatially continuous ET estimates spanning continental to global extents (Allen et al., 2007; Fisher et al., 2008; Mu et al., 2011; Purdy et al., 2018; Martens et al., 2017).

ET is a function of the amount of water in the soil, the atmospheric demand for water, and the incoming solar radiation (Zhang et al., 2016a, 2016b). Many RS ET models use surface energy balance methods for estimating ET over continental to global domains, employing satellite observations of vegetation with spatially gridded surface meteorology as model drivers (Mu et al., 2007; Mu et al., 2011; Purdy et al., 2018). Although many existing RS ET methods implicitly account for the effect of soil moisture on ET through proxy or correlated variables such as atmospheric vapor pressure deficit (VPD) or soil temperature, few methods actually use soil moisture as a model input (Allen et al., 2007; Fisher et al., 2008; Mu et al., 2007; Mu et al., 2011). For example, in the Moderate Resolution Imaging Spectroradiometer (MODIS) MOD16 algorithm, soil evaporation and transpiration are constrained by daily VPD, relative humidity (RH) and minimum air temperature (Tmin; Mu et al., 2007; Mu et al., 2011), based on the assumption of congruence between near surface atmosphere and soil moisture conditions at coarser spatial and temporal scales (Fisher et al., 2008). However, the relationship between VPD and soil moisture can become decoupled at shorter (daily to weekly) time scales, leading to model error (Novick et al., 2016; Purdy et al., 2018). Additionally, many RS ET models do not account for the influence of soil moisture on transpiration, despite the strong relationship between soil water and canopy stomatal conductance (Lu et al., 2011; Novák et al., 2005; Wu et al., 2011; Short Gianotti et al., 2019). Instead, VPD and temperature are generally used to constrain transpiration (Fisher et al., 2008; Mu et al., 2011). However, the lack of soil moisture information neglects a fundamental water balance control on ET, which can lead to significant model error (Michel et al., 2016; Miralles et al., 2016; McCabe et al., 2016).

Here, we introduce a new RS ET model that uses surface and root zone soil moisture information from the NASA Soil Moisture Active Passive (SMAP) mission (Section 4.2.1; Reichle et al., 2019) as a control on estimated soil evaporation and transpiration (Section 3.1). The model is built using the MOD16 framework (Section 2.1; Mu et al., 2007; Mu et al., 2011), which uses the Penman-Monteith method for estimating ET and is one of the only global operational RS ET products. The objectives of this study are to (i) investigate the influence of the introduced soil moisture control on the model ET estimates; and (ii) determine where and why the added soil moisture information is more influential. The following sections describe the baseline MOD16 algorithm (Section 2); the model enhancements and methods used for evaluating soil moisture related impacts on ET, and the model calibration and validation (Section 3); a summary of the study area, and the materials and data used as

model inputs (Section 4); followed by a presentation of the model results (Section 5), significance (Section 6), and major conclusions (Section 7) from this study.

2. Theoretical background

2.1. MOD16 algorithm

MOD16 uses coarse (approximately 55 km \times 70 km) global surface meteorology inputs from the Goddard Earth Observing System (GEOS) Forward Processing for Instrument Teams (FP-IT) product (Rienecker et al., 2008; Lucchesi, 2015) and MODIS Collection 6 surface reflectance products within a modified Penman-Monteith algorithm to estimate daily ET (Mu et al., 2011). The NASA MODIS MOD16 operational processor aggregates the daily model outputs to a coarser 8-day temporal average to produce the final ET global product at a 500 m spatial resolution. The MOD16 algorithm has nine parameters that influence ET environmental response characteristics for different plant functional type (PFT) classes defined from a model Biome Properties Look-up Table (BPLUT; Table S1). The model BPLUT parameters are defined for 11 unique PFT categories represented by the MODIS MOD12Q1 (Type 2) global land cover product. The model BPLUT is applied with spatially varying land cover, vegetation cover, and daily meteorology to predict spatial and temporal variability in ET over the global domain. The core MOD16 algorithm calculates the latent energy (λE , W m⁻²) form of ET as:

$$\lambda E = \frac{s \cdot A + \rho \cdot C_p \cdot VPD/r_a}{s + \gamma \cdot \left(1 + \frac{r_s}{r_a}\right)} \tag{1}$$

where s is the slope of the saturated water vapor pressure curve with respect to temperature (Pa K⁻¹); A is the available incoming energy (Wm⁻²); ρ is the air density (kg m⁻³); C_p is the specific heat capacity of air (J kg⁻¹ K⁻¹); VPD is the vapor pressure deficit (Pa); r_s and r_a are the surface and aerodynamic resistances to ET, respectively (s m⁻¹), and γ is the psychrometric constant (Pa K⁻¹). MOD16 further partitions ET into its three major components: evaporation from the wet plant canopy (λE_{WC} ; W m⁻²), transpiration through plant stomata (λE_{TRANS} ; W m⁻²), and soil evaporation (λE_{EVAP} ; W m⁻²), such that:

$$\lambda E_{TOTAL} = \lambda E_{WC} + \lambda E_{TRANS} + \lambda E_{EVAP}.$$
 (2)

Sections 2.1.1 and 2.1.2 further describe λE_{TRANS} and λE_{EVAP} , which were both modified in the updated algorithm (Section 3.1). Since λE_{WC} is unaffected by soil moisture, it is not modified in the updated algorithm and the reader is referred to section 2.7 of Mu et al. (2011) for details.

2.1.1. Plant transpiration calculation

The λE_{TRANS} term in the MOD16 algorithm builds on Eq. (1) by partitioning incoming solar radiation to the dry plant canopy:

$$\lambda E_{TRANS} = \frac{(1 - Fwet) \cdot F_c \cdot (s \cdot A_c + \rho \cdot Cp \cdot VPD/r_a)}{s + \gamma \cdot (1 + r_s/r_a)}$$
(3)

$$Fwet = \begin{cases} 0 & RH < 70\% \\ \left(\frac{RH}{100}\right)^4 & 70\% \le RH \le 100\% \end{cases}$$
 (4)

where A_C is the available incoming energy at top of canopy (W m⁻²); F_C is the fractional canopy cover of a pixel (dimensionless); *Fwet* is the fraction of the canopy that is wet (%; Fisher et al., 2008), and RH is the relative air humidity (%). r_s is a key driver of transpiration, as it is partially controlled by the leaf stomatal conductance, which ultimately determines canopy transpiration. r_s is calculated as the inverse of canopy-level conductance (C_C ; s m⁻¹):

$$r_s^{-1} = C_c = \frac{gl_{sh} \cdot (G_s + G_{CU})}{G_s + gl_{sh} + G_{CU}} \cdot LAI \cdot (1 - Fwet)$$
 (5)

$$G_{CU} = 0.00001 \cdot r_{corr} \tag{6}$$

$$r_{corr} = \frac{1}{\frac{101300}{P_a} \cdot \left(\frac{T}{293.15}\right)^{1.75}} \tag{7}$$

$$G_s = C_L \cdot m(Tmin) \cdot m(VPD) \cdot r_{corr}$$
(8)

$$m(T_{min}) = \begin{cases} 1 & T_{min} \ge T_{minopen} \\ \frac{T_{min} - T_{minclose}}{T_{minopen} - T_{minclose}} & T_{minclose} < T_{min} < T_{minopen} \\ 0 & T_{minclose} \end{cases}$$
(9)

$$m(VPD) = \begin{cases} 1 & VPD \leq VPD_{open} \\ \hline VPD_{close} - VPD & VPD \leq VPD_{open} \\ \hline VPD_{close} - VPD_{open} & VPD \leq VPD_{close} \\ 0 & VPD \geq VPD_{close} \end{cases}$$
(10)

where $g\underline{l}.sh$ is the leaf conductance to sensible heat per unit leaf area index (LAI; s m $^{-1}$); G_S is the stomatal conductance per unit LAI (s m $^{-1}$); G_{CU} is the leaf cuticular conductance (s m $^{-1}$); and r_{corr} is a function that corrects the conductance according to local air temperature T (K) and pressure P_a (Pa). To calculate G_S , the potential rate of transpiration per unit LAI (G_L ; s m $^{-1}$) is scaled using two linear ramp functions, $m(T_{min})$ and m(VPD), and the r_{corr} term. The ramp functions produce a dimensionless scalar value ranging between zero and unity for respective fully constrained (value = 0) and unconstrained (value = 1) stomatal conductance to water loss. This functional representation assumes that plants both fully open ($T_{minopen}$, VPD_{open}) and close ($T_{minclose}$, VPD_{close}) their stomata under optimal and adverse environmental conditions (Jones et al., 2017; Mu et al., 2007). The product of the scalars accordingly reduces stomatal conductance (G_S) from its prescribed maximum rate (G_L) for different PFT classes.

2.1.2. Soil evaporation calculation

Soil evaporation is derived from the sum of saturated (λE_{SAT}) and non-saturated (λE_{nSAT}) soil surfaces within a pixel:

$$\lambda E_{SAT} = \frac{Fwet \cdot \left(s \cdot A_{SOIL} + \rho \cdot C_p \cdot (1 - F_C) \cdot VPD/r_{as}\right)}{s + \gamma \cdot r_{tot}/r_{as}}$$
(11)

$$\lambda E_{nSAT} = \frac{(1 - Fwet) \cdot (s \cdot A_{SOIL} + \rho \cdot C_p \cdot (1 - F_C) \cdot VPD/r_{as})}{s + \gamma \cdot r_{tot}/r_{as}}$$
(12)

where A_{SOIL} is the fraction of incoming solar radiation available at the soil surface (W m $^{-2}$; Mu et al., 2011); r_{as} is the aerodynamic resistance at the soil surface (s m $^{-1}$); and r_{tot} is the total aerodynamic resistance to water vapor transport (s m $^{-1}$). r_{tot} is assumed to change according to PFT, and is bound by minimum and maximum total aerodynamic resistance BPLUT parameters (rbl_{min} and rbl_{max} ; s m $^{-1}$):

$$r_{tot} = r_{totc} \cdot r_{corr} \tag{13}$$

$$r_{totc} = \begin{cases} rbl_{max} & VPD \leq VPD_{open} \\ rbl_{max} - \frac{(rbl_{max} - rbl_{min}) \cdot (VPD_{close} - VPD)}{VPD_{close} - VPD_{open}} & VPD \leq VPD_{open} < VPD < VPD_{close} \\ rbl_{min} & VPD \geq VPD_{close} \end{cases}$$

Total soil evaporation is calculated as the sum of evaporation from the saturated and unsaturated soil components within a pixel:

 Table 1

 Descriptions of ET models setups evaluated in this study.

Model	Description
ET _{MOD16G}	Baseline MOD16 operational product forced with coarse (approximately $55 \text{ km} \times 70 \text{ km}$) global (G) surface meteorology inputs from the GEOS FP-IT product.
ET_{NSR}	MOD16 algorithm forced with 4 km Gridmet meteorology (Section 4.2.3) with no soil moisture (NS) control, and recalibrated BPLUT parameters that reflect the new regional (R) meteorology inputs.
ET _{NRR}	Updated MOD16 algorithm forced with 4 km Gridmet meteorology and NRv7.2 (Section 4.2.1) soil moisture (NR), and recalibrated BPLUT parameters that reflect the new regional (R) meteorology and soil moisture inputs.
$\mathrm{ET}_{\mathrm{L4R}}$	As in ET $_{\rm NRR}$ but using SMAP L4_SM (Section 4.2.1) as the model soil moisture input (L4).

$$\lambda E_{EVAP} = \lambda E_{SAT} + \lambda E_{nSAT} \cdot f(SM) \tag{15}$$

$$f(SM) = \left(\frac{RH}{100}\right)^{VPD/\beta} \tag{16}$$

where f(SM) is an estimated soil moisture constraint on evaporation that uses RH and VPD as proxies for soil moisture, and β is the soil moisture sensitivity to VPD. f(SM) is a unitless scalar, ranging between zero and unity, defining how much water in unsaturated soil can be lost to evaporation (Fisher et al., 2008).

3. Methods

Our model builds on the MOD16 algorithm outlined in Section 2.1 by introducing two new functions that use SMAP soil moisture (Section 4.2.1) to constrain soil evaporation (Section 3.1.1) and transpiration (Section 3.1.2). Unlike the MOD16 global product, this study is restricted to the contiguous US (CONUS) domain (Section 4.1) and exploits finer regional meteorology inputs from Gridmet (Section 4.2.3). The updated model was calibrated using ET observations from 69 CONUS flux tower sites (Section 4.3), whereas the original model was calibrated using 46 global tower sites. Four different model versions were compared to distinguish impacts from model recalibration, the addition of a soil moisture control, and the use of SMAP observations on model accuracy (Table 1).

3.1. Implementing a soil moisture control on model ET estimates

Here, a modified ET algorithm is implemented, augmenting the baseline MOD16 framework. The enhancements are summarized below and include the addition of surface and root zone soil moisture as additional water supply controls on soil evaporation and transpiration calculations, respectively. This new framework is designed to exploit operational satellite soil moisture information from the NASA SMAP mission.

3.1.1. Soil moisture control on soil evaporation

The *f(SM)* relationship in Eq. (16) assumes that VPD and RH are effective proxies for soil moisture controls on ET (Fisher et al., 2008). However, this assumption may be invalid at the MOD16 daily time scale (Novick et al., 2016) and can contribute to model uncertainty. Here, we replace *f(SM)* in Eq. (15) with a more direct soil moisture control outlined in Fisher et al. (2008):

$$REW = \frac{SFSM - SFSM_{min}}{SFSM_{max} - SFSM_{min}} \tag{17}$$

where *REW* is the relative extractable soil water; *SFSM* is the surface soil moisture of a pixel; and $SFSM_{min}$ and $SFSM_{max}$ are the respective minimum and maximum surface soil moisture values for the period of record. REW is a relative soil moisture index, which assumes that the full range

(14)

of soil moisture variability at a given location is represented within the period of record defined from soil moisture observational inputs.

3.1.2. Soil moisture control on plant transpiration

Previous studies indicate an approximate relationship between transpiration and soil moisture that asymptotes above a maximum threshold where transpiration is insensitive to wetter soil conditions (Gardner and Ehlig, 1963; Novák et al., 2005; Purdy et al., 2018; Short Gianotti et al., 2019; Wu et al., 2011). The transpiration response to soil moisture is represented by the following ramp function, which is similar to the functional form of the model G_S response to VPD and T_{min} (Eq. 8):

$$m(SM) = \begin{cases} \frac{1}{SM_{close} - RZSM} & RZSM \ge SM_{open} \\ \frac{SM_{close} - SM_{open}}{SM_{open} > RZSM > SM_{close}} & RZSM \le SM_{close} \end{cases}$$
(18)

where SM_{close} and SM_{open} are the root zone soil moisture contents at which plants completely close and open their stomata, respectively, and RZSM is the root zone soil moisture scaled between zero and one as described in Eq. (17). m(SM) is used with the VPD and T_{min} scalars in Eq. (8) to determine the bulk model G_S response. The slope and intercept of this relationship varies according to plant type, soil properties, and the rate of transpiration (Novák et al., 2005; Wu et al., 2011); therefore, unique SM_{close} and SM_{open} values were calibrated for different PFT classes and represented within the BPLUT (Section 3.1.3; Table S2). The above MOD16 modifications distinguish atmospheric moisture deficit and soil water supply controls on transpiration and soil evaporation, potentially improving model accuracy and clarifying underlying controls on ET.

3.1.3. Model calibration and ET validation

To accommodate the added model soil moisture control and Gridmet meteorology, we recalibrated the original MOD16 BPLUT parameters (Table S1). However, $T_{minopen}$ and $T_{minclose}$ were left unchanged, as the model performance is insensitive to these parameters (Zhang et al., 2019b). Following Zhang et al. (2019b), we used Differential Evolution Markov Chain Monte Carlo simulations to minimize root mean squared error (RMSE) differences between the model simulations and daily ET observations from tower sites representing major PFT classes.

The calibration procedure was performed 10 times for each PFT, as data were randomly split into 10 equally sized groups for k-fold cross validation. In this process, nine groups were used to calibrate the model parameters, while the remaining holdout group was used to calculate error metrics using the new parameter values. This process was repeated 10 times so that all tower site records could be used for both calibration and validation. The error metrics reported in Table 3 were calculated using all tower data withheld from calibration from 2015 to 2017. This process ensured that all models were compared against the same set of observations, as the $\rm ET_{L4R}$ data were unavailable until after the SMAP launch in 2015. Tower ET observations from 2015 to 2017 were selected from the Ameriflux network (https://ameriflux.lbl.gov) to represent all major CONUS PFT classes, except for DNF, EBF, MF and SAV classes, which did not have suitable tower observations meeting the defined data quality threshold (Section 4.3).

To distinguish improvements in model accuracy contributed from the addition of a new soil moisture control versus recalibration, separate calibrations were performed for ET_{NRR} and ET_{NSR} . The calibrated BPLUT parameters (Tables S2, S3) show the mean values and standard deviations of the parameters that produced the lowest errors for ET_{NRR} and ET_{NSR} , respectively. Parameters defined for ET_{NRR} were also used for ET_{L4R} due to the shorter (2015–2017) SMAP operational record.

To quantify model performance and investigate the role of soil moisture on the ET estimates, all models introduced in Section 3 were compared to daily tower ET observations not used in calibration for the 2015–2017 period using RMSE, bias (model minus observation) and the

coefficient of determination (R^2) as performance metrics. The relative improvements from the novel components of the updated algorithm were assessed for

- (i) the model recalibration and regional Gridmet meteorology (by comparing ET_{MOD16G} and ET_{NSR} ; Section 5.1);
- (ii) the added soil moisture control (by comparing ET_{NSR} and ET_{NRR} ; Section 5.1); and
- (iii) the assimilation of SMAP observations (by comparing ET_{NRR} and ET_{L4R} ; Section 5.2).

3.2. Determining regional influence of soil moisture on model ET estimates

We compared differences in estimated annual average ET from the different model versions over the CONUS domain to determine where the added soil moisture control is more influential on the model ET calculations. Mean annual differences between ET_{L4R}, ET_{NSR}, and ET_{NRR} were used to evaluate the respective impacts of the added soil moisture control and SMAP observations on the model ET estimates. The above comparisons were conducted for the period overlapping with SMAP operations (2015–2017).

The aggregated annual ET results from the models were evaluated against alternative annual ET estimates from the spatially continuous FLUXCOM monthly record (Section 4.4). Here, ET_{NRR} was used as a proxy for ET_{L4R} because it spanned the entire FLUXCOM record (2003–2013). Variations in model ET differences and relative performance against the FLUXCOM ET benchmark were evaluated across the CONUS domain and regional gradient in climate aridity, AI, defined as the ratio of mean annual potential ET to precipitation (United Nations Educational, Scientific and Cultural Organization (UNESCO), 1979).

The partitioning of ET into its primary components (transpiration, soil evaporation and evaporation from the wet canopy) is an important and developing area of study (Fisher et al., 2017). Here, we used the model outputs to map regional differences in the relative contributions of each component to mean annual ET over the CONUS domain. Differences between the ET_{L4R} and ET_{NSR} outputs were used to clarify the spatial influence of SMAP defined soil moisture controls on model ET partitioning. The relative contributions of transpiration, soil evaporation and evaporation from the wet canopy on the aggregate ET calculations were represented by a linear mapping of the relative contribution (%) of each component to total ET. Additionally, we ran the ET_{L4R} model at three flux towers with and without the environmental constraint scalars in Eq. (8) to assess how transpiration is affected by VPD, temperature, and soil moisture across an AI gradient.

4. Study area and materials

4.1. Study area

This study encompasses all CONUS vegetated land areas from 2003 to 2017. The distribution of the dominant PFT classes over the domain is shown in Fig. 1. The CONUS domain contains all 12 PFT classes depicted in the MODIS MCD12Q1 global land cover classification (Friedl et al., 2002), including croplands (broadleaf (BRO) and cereal (CER)), evergreen needleleaf forest (ENF), evergreen broadleaf forest (EBF), deciduous needleleaf forest (DNF), deciduous broadleaf forest (DBF), mixed forest (MF), closed shrubland (CSH), open shrubland (OSH), woody savanna (WSA), savanna (SAV), and grassland (GRA). However, the EBF, DNF, and CSH classes are sparse compared to other PFT categories, with each class representing <1% of the CONUS domain. Additionally, there were no tower observations representing DNF or SAV that met our tower quality (QA/QC) threshold. Therefore, BPLUT parameter values for the DNF and SAV PFT classes were defined from respective ENF and WSA parameters following Mu et al. (2011).

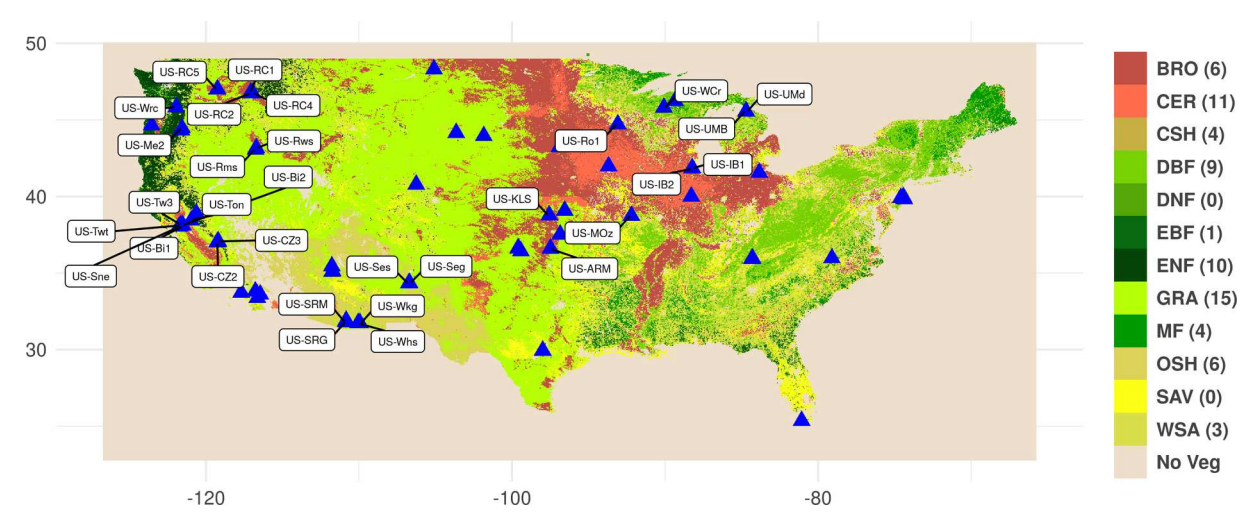


Fig. 1. CONUS land cover derived from the MOD12Q1 Type 2 and Type 5 land cover products for the 2003–2017 period. Blue triangles show the location of AmeriFlux towers used for calibration and validation of new ET models. The labelled towers contain data after March 31st, 2015 that were used for model validation. The number of towers in each PFT class are shown in the legend (in parenthesis). (For interpretation of the references to colour in this figure legend, the reader is referred to the web version of this article.)

4.2. Model inputs

All input datasets used for the model ET calculations are summarized in Table 2. The ET model inputs come from three sources: MODIS surface reflectance products, SMAP soil moisture products, and Gridmet meteorology. MODIS products define land vegetation and surface reflectance characteristics, while SMAP and Gridmet are used to define soil moisture and meteorological constraints on ET, respectively. Input datasets with a temporal resolution greater than one day were linearly interpolated to a daily time step. Sub-daily inputs were aggregated to a daily time step by taking the mean of all values within a day. We resampled all model geospatial inputs to a 500 m resolution using bilinear interpolation to match the MODIS MODI6 operational product (Mu et al., 2011; Zhao et al., 2005). MODIS inputs affected by clouds or atmospheric interference were identified using the respective product quality (QA/QC) flags.

Table 2 All inputs used to model daily ET from the MOD16 algorithm framework used in this study.

Product	Description/Purpose	Spatial Resolution	Temporal Resolution	
SMAP L4_SM	Daily surface and root zone soil moisture inputs from version 4 of the SMAP L4_SM operational product, 2015–2017. Used to drive ET _{L4R} model.	$9 \text{ km} \times 9 \text{ km}$	3-h	
SMAP NRv7.2	Daily surface and root zone soil moisture inputs from SMAP L4_SM Nature Run version 7.2 (NRv7.2), 2003–2017. Used to drive ET _{NRR} model.	9 km × 9 km	3-h	
MCD12Q1	MODIS annual land cover product used to define pixel-level BPLUT values.	500 m × 500 m	Annual	
MCD15A2	MODIS FPAR/LAI product used to partition pixel-level ET between transpiration and evaporation and scale leaf-level transpiration to the canopy.	500 m × 500 m	4-day	
MCD43A3	MODIS surface albedo product used to determine net solar radiation available for ET.	500 m × 500 m	Daily	
Gridmet	Daily meteorological inputs to the ET model, including maximum and minimum temperature, VPD, RH and incoming solar radiation.	$4 \text{ km} \times 4 \text{ km}$	Daily	

Affected pixels were gap-filled using temporal nearest-neighbor selection of adjacent good pixel values (Zhao et al., 2005). We developed and ran the model on the Google Earth Engine (GEE) platform (Gorelick et al., 2017) and summarized model results using the R programming language.

4.2.1. SMAP L4 SM soil moisture

We used version 4 of the NASA SMAP mission operational Level-4 Soil Moisture product (L4_SM; Reichle et al., 2018) as model surface and root zone soil moisture inputs. The L4_SM product is derived from the global assimilation of SMAP L-band (1.4GHz) daily microwave brightness temperature (Tb) observations into the NASA Catchment land surface model (CLSM; Koster et al., 2000). The L4_SM model uses an ensemble Kalman filter to assimilate SMAP brightness temperatures and other observations into the CLSM for estimating surface (top 5 cm) and root zone (0-1 m depth) soil moisture (Reichle et al., 2017a). Unlike lower order satellite retrievals, the L4_SM product is spatially and temporally continuous over the global domain and includes model informed calculations of root zone soil moisture conditions that are consistent with the assimilated SMAP brightness temperature observations.

The SMAP L4_SM operational product is available starting March 31st, 2015, which limits how far back we can derive the ET_{L4R} record. This relatively short record can misrepresent the longer-term soil moisture climatology required by the ET model (e.g. Eqs. 17, 18). The operational record also imposes a temporal discontinuity between model drivers and tower ET observations used for model calibration and validation; whereby, the bulk of available tower observations occur prior to 2015 (e.g. FLUXNET2015; Pastorello et al., 2017), with sufficient measurements available for this study through 2017, which leaves us with an approximately three-year study period (2015–2017).

To address the above limitations, we extended the model ET simulations over a longer record (2003–2015) using the SMAP Nature Run version 7.2 (NRv7.2) soil moisture product (Reichle et al., 2019). NRv7.2 is derived from the same CLSM version as the L4_SM product but is not informed by SMAP observations. In a ground validation study of 18 sites spanning various climate and PFT conditions, NRv7.2 estimated surface (root zone) soil moisture with an unbiased RMSE of 0.043 $\rm m^3 m^{-3}$ (0.030 $\rm m^3 m^{-3}$), and the assimilation of SMAP Tb observations improved the unbiased RMSE to 0.039 $\rm m^3 m^{-3}$ (0.026 $\rm m^3 m^{-3}$) for L4_SM (Reichle et al., 2019). This accuracy is sufficient for representing soil moisture related controls within our ET model framework. Both L4_SM

and NRv7.2 produce global estimates of surface and root zone soil moisture at a 3-h time step on the 9 km resolution global EASE-grid (version 2; Brodzik et al., 2014). We used the L4_SM (and NRv7.2) root zone soil moisture estimates to constrain transpiration and the corresponding surface soil moisture estimates to constrain soil evaporation in the model ET calculations.

4.2.2. MODIS products (collection 6)

The MODIS MCD15A3H product (Myneni et al., 2002) provides composited global estimates of LAI and FPAR every four days at a 500 m resolution. The LAI/FPAR product is used in MOD16 to partition incoming solar radiation between the soil surface and plant canopy. FPAR serves as a proxy for fractional vegetation cover (F_C) within a pixel (Eq. 3), while LAI is used to upscale leaf stomatal conductance to canopy-level conductance (Eq. 5). The MODIS MCD43A3 Albedo product (Schaaf and Wang, 2015) provides global daily 500 m surface albedo

estimates, which are used to derive daily net radiation from incoming shortwave radiation, consistent with the baseline MOD16 logic.

The MODIS MCD12Q1 land cover product (Friedl et al., 2002) gives the dominant PFT within each 500 m pixel and is used to assign BPLUT parameters to each pixel. The original MOD16 logic uses the MODIS MCD12Q1 Type 2 land cover classification, which does not distinguish BRO and CER crop types. However, BRO and CER account for approximately 4.6% and 14.1% of the CONUS domain, respectively. Here, we use a combination of the Type 2 and Type 5 land cover schemes to better distinguish ET conditions between the two crop types. For a given pixel, if the Type 2 PFT is classified as cropland and the Type 5 value represents either BRO or CER, we assign the pixel to the appropriate Type 5 category.

4.2.3. Gridmet meteorology

The MODIS MOD16 operational product uses GEOS FP-IT input

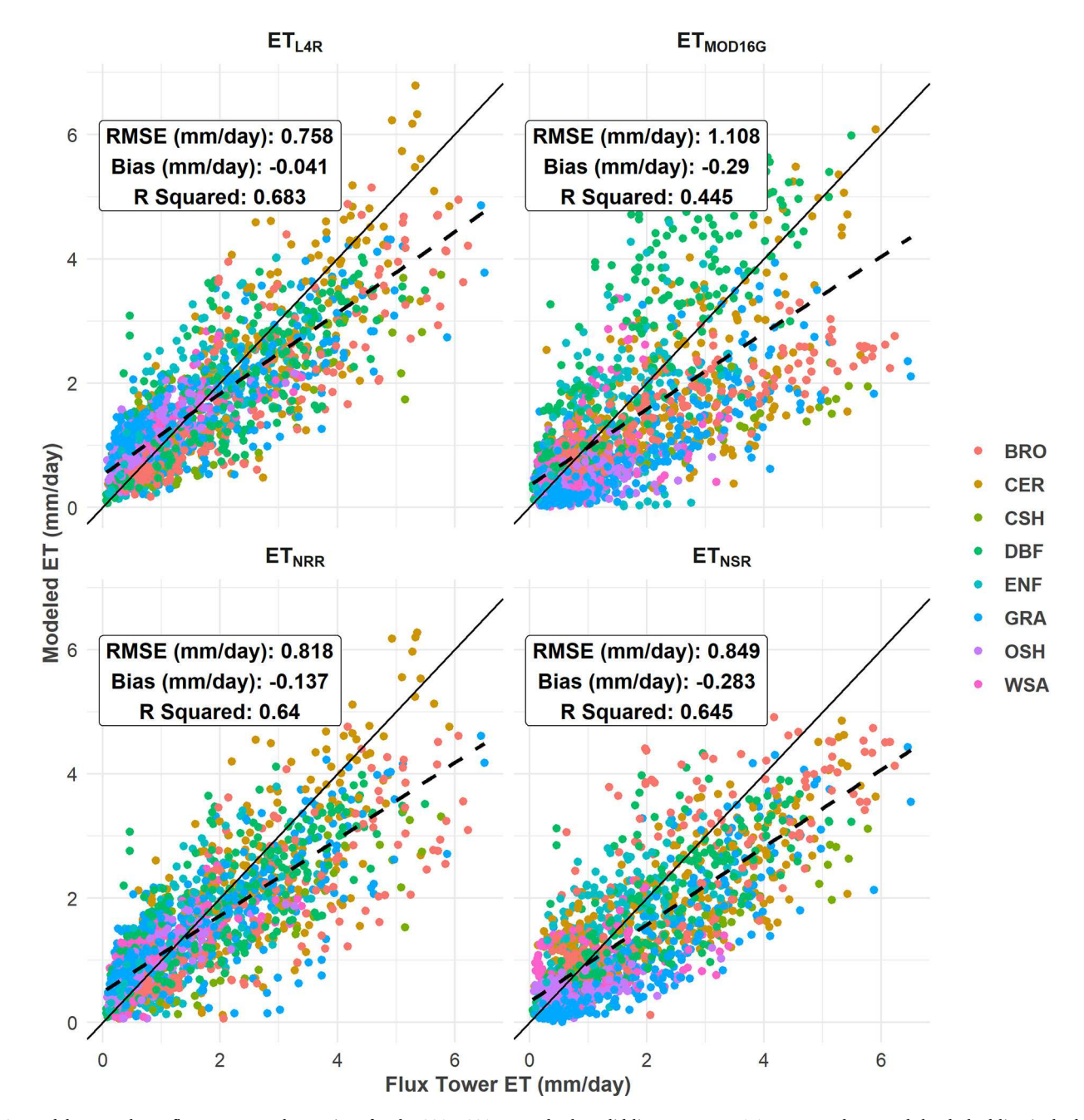


Fig. 2. Model ET results vs flux tower ET observations for the 2015–2017 record. The solid line represents 1:1 correspondence and the dashed line is the best-fit linear regression line for each ET model.

Table 3Results of model performance using holdout ET validation data from 31 flux towers for the 2015–2017 record. Bias is the mean daily difference between model and tower ET observations (model – observation; mm day⁻¹).

PFT	ET_{L4R}			ET _{NRR}			ET _{NSR}			ET_{MOD16G}		
	Bias	\mathbb{R}^2	RMSE	Bias	\mathbb{R}^2	RMSE	Bias	\mathbb{R}^2	RMSE	Bias	\mathbb{R}^2	RMSE
BRO	-0.668	0.703	1.117	-0.804	0.624	1.297	-0.183	0.546	1.127	-1.103	0.714	1.567
CER	-0.047	0.72	0.771	-0.136	0.644	0.887	-0.328	0.615	0.965	-0.401	0.472	1.17
CSH	-0.654	0.716	1.134	-0.766	0.733	1.201	-0.833	0.936	1.23	-1.14	0.787	1.644
DBF	-0.09	0.632	0.836	-0.086	0.646	0.823	-0.233	0.681	0.809	0.824	0.679	1.251
ENF	0.058	0.583	0.592	-0.099	0.504	0.627	0.185	0.435	0.652	-0.045	0.296	0.863
GRA	-0.009	0.693	0.747	-0.068	0.604	0.833	-0.635	0.783	0.893	-0.643	0.59	1.069
OSH	0.334	0.513	0.521	0.087	0.626	0.365	-0.203	0.291	0.54	-0.369	0.22	0.635
WSA	0.191	0.607	0.5	0.165	0.545	0.522	-0.104	0.201	0.668	-0.11	0.212	0.759
Average	-0.041	0.683	0.758	-0.137	0.64	0.818	-0.283	0.645	0.849	-0.29	0.445	1.108

 R^2 is the coefficient of determination describing correspondence between the selected model and associated flux tower measurements. RMSE is the root mean squared error difference between model estimates and tower observations (mm day $^{-1}$). Bold values denote the best performing model for each metric and PFT. The 'Average' row is the value of each metric calculated across all flux tower observations from 2015 to 2017.

meteorology for the ET calculations. Here, we use an alternative Gridmet daily surface meteorology record (Abatzoglou, 2013) as inputs for the model ET calculations. Although Gridmet is limited to the CONUS, it has a smaller pixel size than the global GEOS FP-IT product (4 km \times 4 km vs 55 km \times 70 km), which may enhance the spatial representation of ET and underlying environmental drivers (He et al., 2019b).

4.3. AmeriFlux ET

We used in situ daily ET observations from the AmeriFlux tower network (Baldocchi et al., 2001) for BPLUT calibration and model ET validation. We followed the gap filling and QA/QC procedure described by Mu et al. (2011) to remove lower quality data and to upscale the 30min tower observations to a daily time step. Additionally, many flux tower observations fail to close the energy balance (Foken et al., 2006; Purdy et al., 2018), which can lead to unrealistic ET estimates. To address this issue, we filtered out any 30-min data where the energy imbalance exceeded 300 W m⁻², following Zhang et al. (2019b). The QA/QC procedure left 69 (of 107 initial sites) representing 10 PFT classes (Table S4). The energy balance closures for the 69 remaining sites ranged from 77 to 92%, suitable for model calibration and validation (Foken et al., 2006; Michel et al., 2016; Zhang et al., 2019b). The regional distribution of tower sites used in this study is presented in Fig. 1, along with a detailed site summary in Table S4. Only 31 tower sites had data available after March 31st, 2015 (beginning of SMAP operational record) that met the above QA/QC procedure. These 31 towers were used for ET validation so that all new models could be compared against a consistent tower record. To compare model estimates to tower observations, mean model ET estimates from a 1 km diameter circle centered at each tower location were compared to the corresponding tower ET observations.

4.4. FLUXCOM

The AmeriFlux observations used for the model ET validation depict dominant biomes within the CONUS domain but are spatially and temporally sparse. To augment the model evaluation, we used the spatially continuous FLUXCOM RS + METEO record (Jung et al., 2019; Tramontana et al., 2016) as an additional validation source. FLUXCOM provides gridded monthly latent heat flux estimates at 0.5° (~55 km) resolution for our entire study period (Jung et al., 2019, Tramontana et al., 2016). The FLUXCOM data are produced through machine learning upscaling of in situ tower observations from the global FLUX-NET synthesis record using MODIS remote sensing and modeled surface meteorological data. FLUXCOM provides latent heat flux estimates suitable for ET model benchmark assessments based on reported high accuracy relative to flux tower observations and good correspondence with various RS ET models (Jung et al., 2019, Tramontana et al., 2016).

Following Jung et al. (2019), we converted FLUXCOM latent heat flux estimates to ET using a constant latent heat of vaporization (2.45 MJ mm⁻¹). We upscaled our 500 m daily ET model results to the coarser FLUXCOM resolution by taking the spatial mean of aggregated monthly ET estimates within each FLUXCOM grid cell. Because FLUXCOM uses flux tower observations as a model input, it is not completely independent from the models evaluated here. However, it still provides a meaningful benchmark spanning the entire CONUS domain and implicitly accounts for PFTs missing from the model tower validation.

5. Results

5.1. Soil moisture influence on model ET estimates

Across all CONUS flux towers, the addition of a soil moisture control improved the accuracy of the model ET estimates. Both ET_{NRR} and ET_{L4R} showed the best performance against the tower ET observations, with respective mean RMSE differences of 0.818 and 0.758 mm d $^{-1}$, and accompanying R 2 agreement of 64.0% and 68.3% (Fig. 2, Table 3). In contrast, the model ET results derived without a direct soil moisture control had generally lower performance and accuracy, including ET_{NSR} (RMSE = 0.849 mm d $^{-1}$; R 2 = 64.5%) and ET_{MOD16G} (RMSE = 1.108 mm d $^{-1}$; R 2 = 44.5%). The relative RMSE improvements between ET_{L4R} and ET_{MOD16G} (11% vs 31%), indicating that recalibration and high resolution (4 km) meteorology are key reasons for improved accuracy and that a soil moisture control further improves model estimates.

Similar results are seen across the eight PFT classes represented from the tower validation sites (Table 3). For all PFTs other than DBF, either ET_{NRR} or ET_{L4R} showed the lowest RMSE values. ANOVA tests comparing all models across all PFTs show that differences between the soil moisture-constrained models and ET_{NSR} are statistically significant, and that with the exception of DBF, CER and WSA PFTs, differences between ET_{NRR} and ET_{L4R} are also statistically significant (Fig. S1). Across the eight PFTs, ET_{NRR} and ET_{L4R} also showed consistently lower bias and higher R^2 correspondence than ET_{NSR} or ET_{MOD16G} (Table 3). Time series ET plots at eight flux tower locations representing seven diverse CONUS PFT classes show that all models track seasonal and annual ET variability across a broad climate and land cover gradient (Fig. 3). In general, ET_{NRR}, ET_{L4R}, and ET_{NSR} better capture the tower observed seasonal variation in ET than the $ET_{\mbox{\scriptsize MOD16G}}$ baseline. These results are also consistent with the majority of PFT classes examined (Table 3). For all PFTs except for DBF, ET_{MOD16G} underestimates the tower ET observations. However, this relationship varies among different tower sites from the same PFT class. For example, ET_{MOD16G} generally underestimates ET across all ENF and WSA tower sites, but overestimates ET at the US-Wrc (ENF) and US-Ton (WSA) sites (Fig. 3). A similar pattern emerges across the CONUS domain, where ET_{MOD16G}

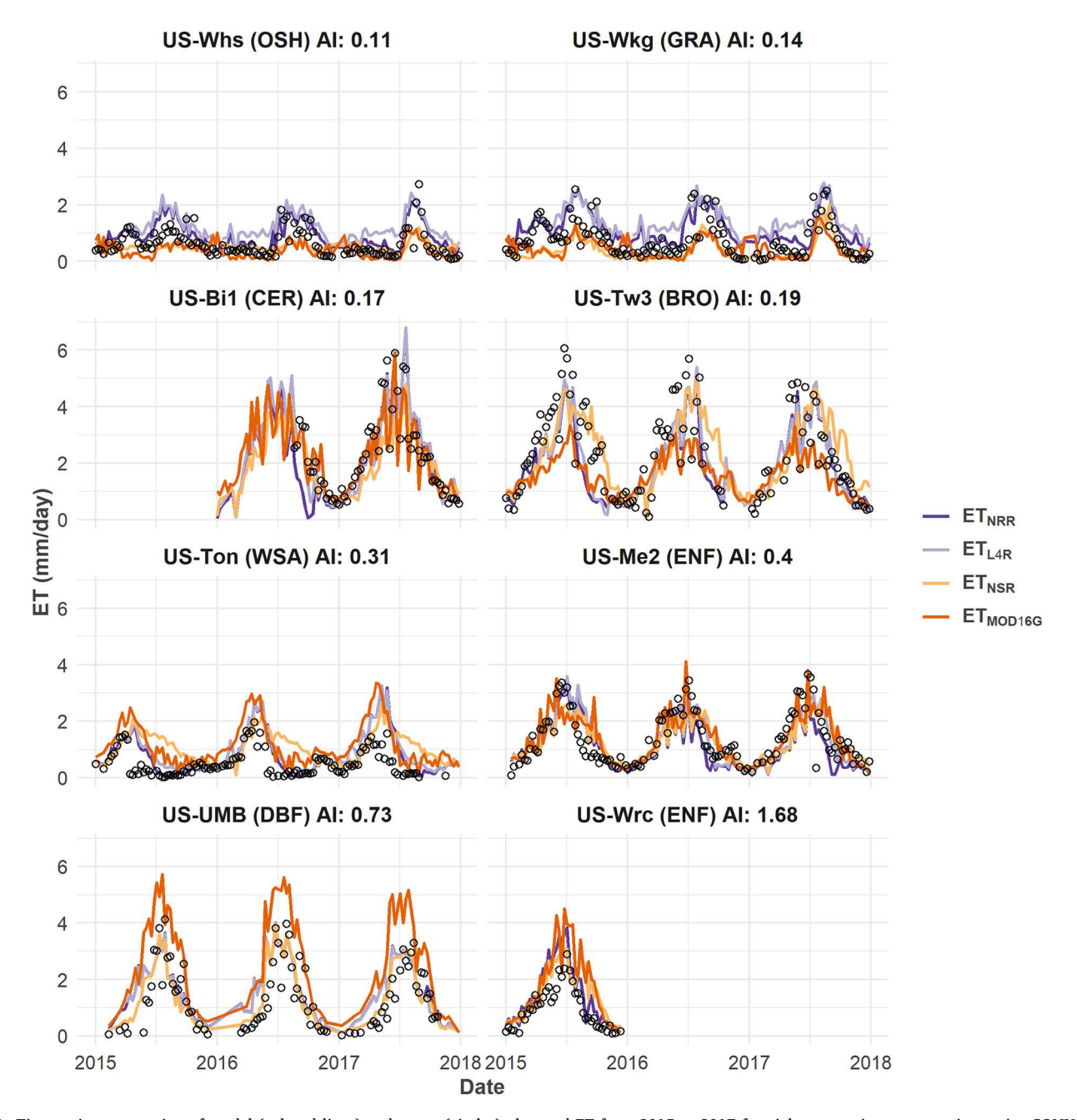


Fig. 3. Time series progression of model (colored lines) and tower (circles) observed ET from 2015 to 2017 for eight tower sites representing major CONUS PFT classes. The aridity index (AI; precipitation / potential ET; UNESCO, 1979) at the sites ranges from arid (0.11; US-Whs) to humid (1.68; US-Wrc). Sites are arranged from most arid to least arid.

predicts higher ET than the soil moisture constrained models for BRO, CRO, DBF, DNF, ENF, MF, SAV and WSA, but lower ET for other PFTs (Fig. 4A). Across the CONUS, median $\rm ET_{NRR}$, $\rm ET_{L4R}$, and $\rm ET_{NSR}$ values fall closer to median flux tower observations, suggesting better ET performance in the updated models relative to the MOD16 baseline (Fig. 4A, B).

The ET_{L4R} results show generally higher and lower ET rates respectively east and west of the 100th meridian (Fig. 5). This same general pattern is seen in all four models (not shown), although ET_{MOD16G} systematically underestimates ET in the western CONUS compared to the updated models. Because the western CONUS is dominated by GRA and OSH (Fig. 1), these results paired with the tower validation assessment (Table 3 and Fig. 3) indicate that ET_{MOD16G} tends to underestimate ET for both of these PFTs and over the western CONUS. Differences between the ET_{NSR} and ET_{L4R} estimates are also more pronounced in the western

CONUS (Fig. 6A), particularly for CSH, GRA, and OSH areas (Fig. 1). In this region, $\rm ET_{NSR}$ predicts generally less ET than $\rm ET_{L4R}$ or the tower observations (Table 3, Fig. 6A).

5.2. Regional influence of soil moisture on model ET estimates

Regional differences between ET_{NRR} and ET_{L4R} reveal the relative impact of the SMAP L-band brightness temperature observations on the L4_SM soil moisture inputs and resulting model ET simulations. The relative value of SMAP observations is greater in the CONUS western dryland regions (Fig. 6B), coinciding with GRA and other PFT classes characterized by low to moderate vegetation cover, where the SMAP soil moisture performance is higher (Reichle et al., 2017a; Reichle et al., 2017b). However, the impact of the SMAP observations on ET, indicated by the ET_{NRR} and ET_{L4R} difference, is smaller than the utility gained from

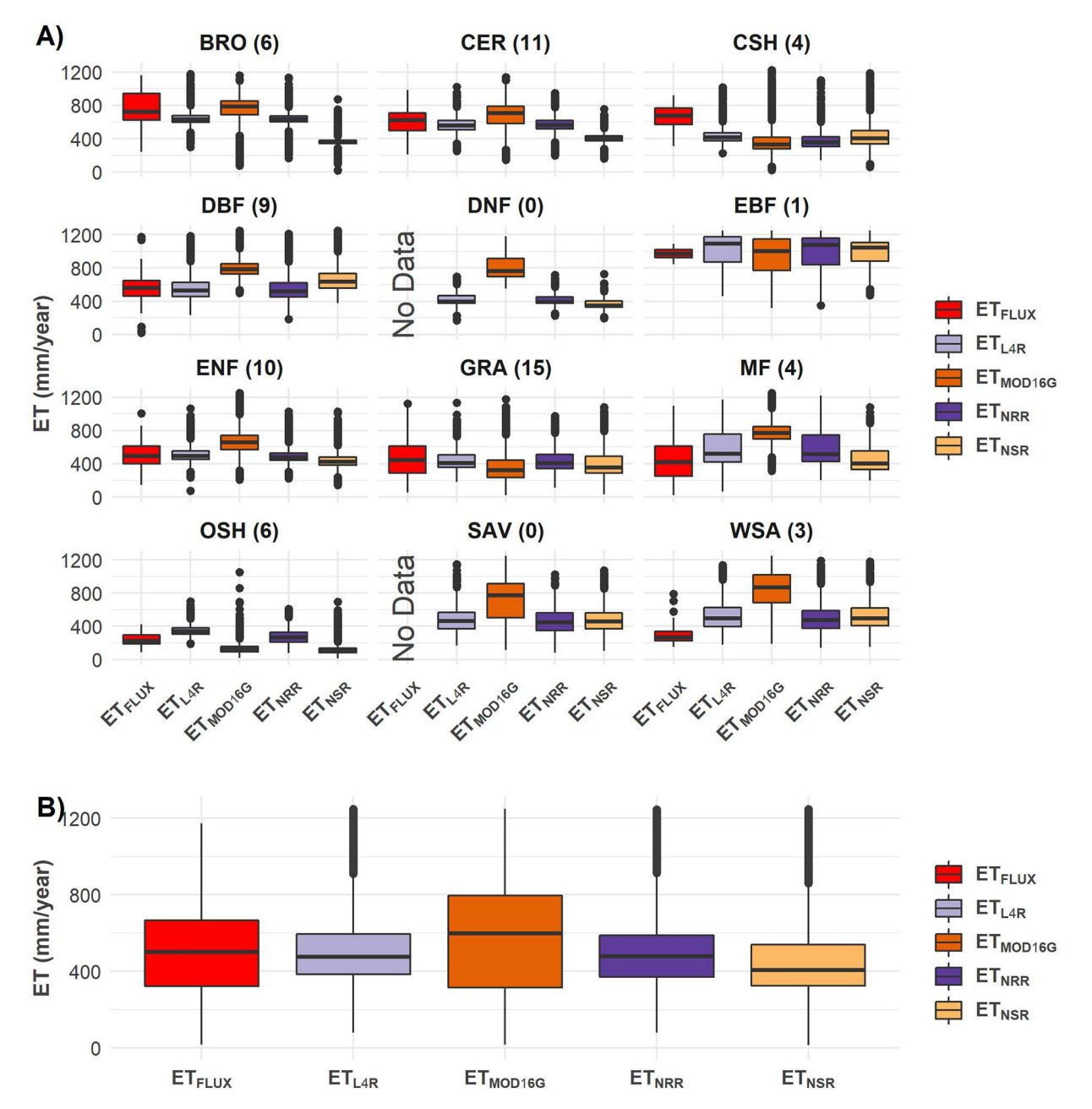


Fig. 4. A) Box plot distributions of modeled ET across all CONUS PFT regions for the 2015–2017 period. Data were plotted by randomly sampling 5000 pixels from each PFT region and aggregating the results for each model. B) Box plot distributions of modeled ET across the entire CONUS domain for the 2015–2017 period. In both plots, associated flux tower observations (ET_{FLUX}) for the same period of record are plotted in red, while the number of towers in each population are shown in parentheses. (For interpretation of the references to colour in this figure legend, the reader is referred to the web version of this article.)

adding a soil moisture control to the model as indicated from the larger and more extensive ET_{L4R} and ET_{NSR} differences (Fig. 6).

When compared to the FLUXCOM estimates, ET_{MOD16G} , ET_{NRR} , and ET_{NSR} all underestimate ET across the CONUS domain, with respective mean annual biases of -145, -168, and -189 mm yr^{-1} . Model performance relative to FLUXCOM varies greatly to the west and east of the 100th meridian (Fig. S2). In the west, ET_{MOD16G} shows an RMSE difference of 211 mm yr^{-1} relative to FLUXCOM, while ET_{NRR} and ET_{NSR} show smaller respective RMSE differences of 130 and 152 mm yr^{-1} . In the east, ET_{MOD16G} is the best performing model in relation to FLUXCOM, with an RMSE difference of 228 mm yr^{-1} , while ET_{NSR} and ET_{NSR} show larger respective RMSE differences of 244 and 258 mm yr^{-1} . Across the CONUS, ET_{NRR} R^2 correspondence relative to FLUXCOM is slightly higher than ET_{NSR} and notably higher than ET_{MOD16G} , particularly in the west (East: $ET_{NRR} = 0.22$, $ET_{NSR} = 0.19$, $ET_{MOD16G} = 0.20$;

West: $ET_{NRR} = 0.40$, $ET_{NSR} = 0.40$, $ET_{MOD16G} = 0.29$).

The model ET performance over the CONUS climate aridity (AI) gradient indicates that ET_{NRR} outperforms both ET_{NSR} and ET_{MOD16G} in more arid regions relative to FLUXCOM (Fig. 7). In the most arid regions, ET_{NRR} has both lower RMSE and lower R² correspondence than the other models (Fig. 7B, C). This relationship shifts after the transition from arid to semi-arid (AI $\sim\!0.4$) climates, where ET_{MOD16G} has a lower RMSE and lower R² relative to FLUXCOM, suggesting that the added soil moisture control has the greatest value for improving the model ET performance in arid and semi-arid regions (AI $\leq\!0.4$) that represent approximately 43% of the CONUS domain. Much of this area falls within the western portion of the domain. The results of the flux tower and FLUXCOM comparisons indicate that the added soil moisture control, represented by ET_{NRR} and ET_{L4R}, produces more realistic model ET estimates in the arid western CONUS region than alternative model simulations derived

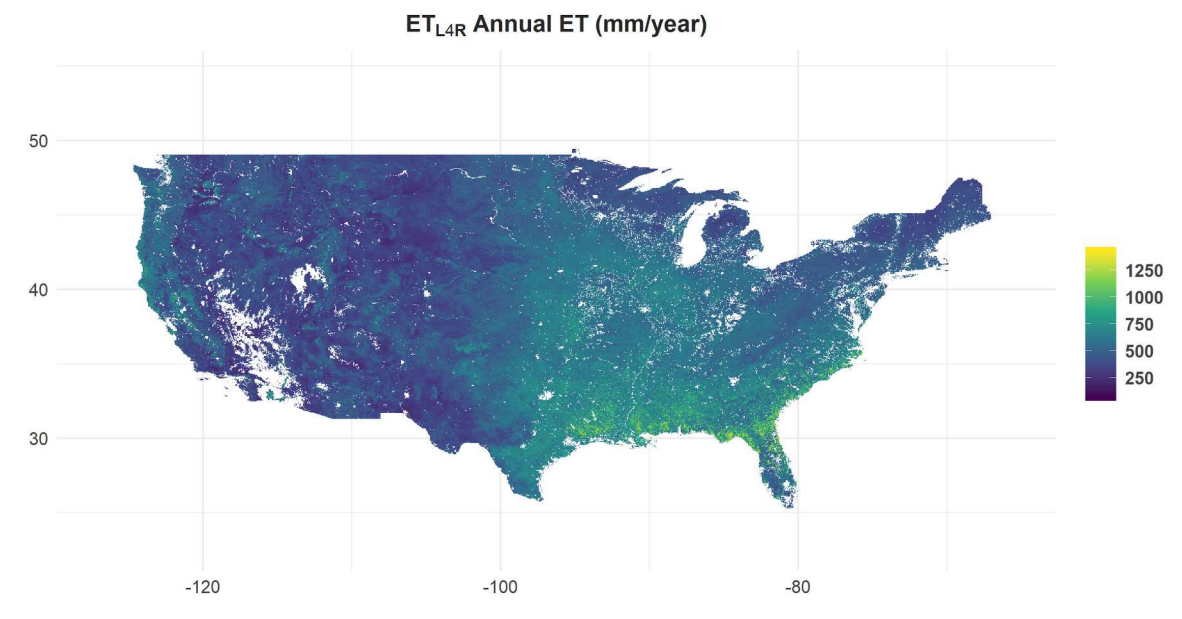


Fig. 5. Spatial pattern of ET_{L4R} across the CONUS domain for the 2015–2017 period, superimposed on a lat/lon grid. White areas represent open water, barren land or other areas external to the modeling domain that were excluded from the ET simulations.

using VPD as the sole moisture control on ET.

Both ET_{L4R} and ET_{NSR} show similar patterns in ET partitioning (soil evaporation, transpiration, wet canopy evaporation) across the domain (Fig. 8). While the models show lower (higher) transpiration contributions in the western (eastern) CONUS, $\mathrm{ET}_{\mathrm{L4R}}$ has notably higher soil evaporation in the west. Across the entire domain, transpiration contributes 44% of ET for ET_{L4R} , and 50% of ET for ET_{NSR} . The difference between the two models is largely driven by partitioning differences east and west of the 100th meridian. In the east, transpiration comprises 50% (52%) of ET_{L4R} (ET_{NSR}), but only 34% (46%) in the west. These results highlight the effect of the added soil moisture control on model ET partitioning. In the more arid regions (i.e. western CONUS), the added soil moisture control leads to greater reduction in transpiration due to the addition of m(SM) in Eq. (18). This effect is illustrated by the difference in ET_{L4R} results derived with and without the environmental constraint scalars (Fig. 9). At the more arid US-Me2 and US-Ton sites, the added soil moisture control reduces transpiration from optimal levels and consequently increases soil evaporation as a percent of ET (Fig. 9). This is not the case at the less arid US-UMB site, where ET is not water limited.

6. Discussion

6.1. Soil moisture influence on model ET estimates

Model calibration and the higher-resolution Gridmet meteorology inputs led to the largest increase in ET accuracy, indicated by larger improvements in ET $_{\rm NSR}$ accuracy over the ET $_{\rm MOD16G}$ baseline compared to improvements in ET $_{\rm NRR}$ and ET $_{\rm L4R}$ over ET $_{\rm NSR}$ (Table 3, Fig. 2). Zhang et al. (2019b) also reported that much of the error in MOD16 could be reduced by a more robust model calibration. They found that across all PFTs, the recalibrated MOD16 RMSE decreased by 28.5%. Similarly, we found a 23.3% RMSE reduction in ET $_{\rm NSR}$ compared to the ET $_{\rm MOD16G}$ baseline by recalibrating the model for the CONUS domain and using Gridmet meteorology. The ET $_{\rm L4R}$ and ET $_{\rm NRR}$ results showed even greater respective RMSE reductions of 31.6% and 26.2% over the ET $_{\rm MOD16G}$ baseline, indicating that the addition of surface and root zone soil moisture controls led to further improvements in model ET accuracy.

The RMSE reductions in ET_{NRR} and ET_{L4R} over ET_{NSR} reflects the addition of explicit soil moisture related controls on model ET. The SM_{close} and SM_{open} parameters in the revised BPLUT represent the unique

role of soil moisture, in addition to VPD, in regulating stomatal conductance (Novick et al., 2016; Novák et al., 2005; Purdy et al., 2018). The calibrated SM_{close} and SM_{open} values fall within the ranges seen in various RS-based productivity models and field studies, suggesting that the parameterization process converged on realistic values for these parameters (Table S2; Wu et al., 2011; He et al., 2016; Jones et al., 2017; Novák et al., 2005). Although some of the SM_{open} parameter values have high standard deviations (i.e. uncertainty), ANOVA test results show that ET_{NRR} and ET_{NSR} estimates are statistically different, suggesting that the model is sensitive to this parameterization and that it drives improvements in ET. Additionally, other MOD16 sensitivity studies have found C_L to be among the most sensitive BPLUT parameters (Zhang et al., 2019b; He et al., 2019b). Here, calibrated C_L values are higher than in the original MOD16 BPLUT, which reflects the added m(SM)control on stomatal conductance described in Section 3.1.2 (Mu et al., 2011).

The higher ET rates modeled by ET_{NRR} and ET_{L4R} were more consistent with the tower observations and previous studies, indicating that MOD16 generally underestimates ET in arid and sparsely vegetated areas (Khan et al., 2018; Michel et al., 2016; Moreira et al., 2019; Ruhoff et al., 2013; Zhang et al., 2020). This bias is most notable in western CONUS grasslands, where ET_{NRR} and ET_{L4R} predict $\sim 100-300$ mm yr⁻¹ more ET than the ET_{MOD16G} baseline (Table 3, Fig. 4). Similarly, Khan et al. (2018) found that MOD16 had an average bias of -104 mm yr⁻¹ across grassland sites in eastern Asia. Across the CONUS domain and 2003–2017 study period, ET_{MOD16G} displayed a - 148 mm yr⁻¹ bias against all GRA tower observations, whereas ET_{NRR} had a positive and much smaller bias of 0.529 mm yr⁻¹. The recalibrated ET_{NSR} and ET_{MOD16G} results both showed markedly lower ET rates in the western CONUS than ET_{NRR}, ET_{L4R}, and the ET benchmarks (both tower observations and FLUXCOM). These results suggest that the baseline MOD16 algorithm is not properly structured to capture the magnitude of ET in arid regions (Figs. 6, 7, S1).

6.2. Regional influence of soil moisture on model ET estimates

Differences in model ET estimates in arid regions follow differences in model partitioning between transpiration and soil evaporation (Fig. 8). In arid regions, canopy gas exchange, including both CO₂ and water vapor, is strongly limited by plant-available soil moisture (Smith et al., 2019), which restricts both vegetation growth and ET. In the

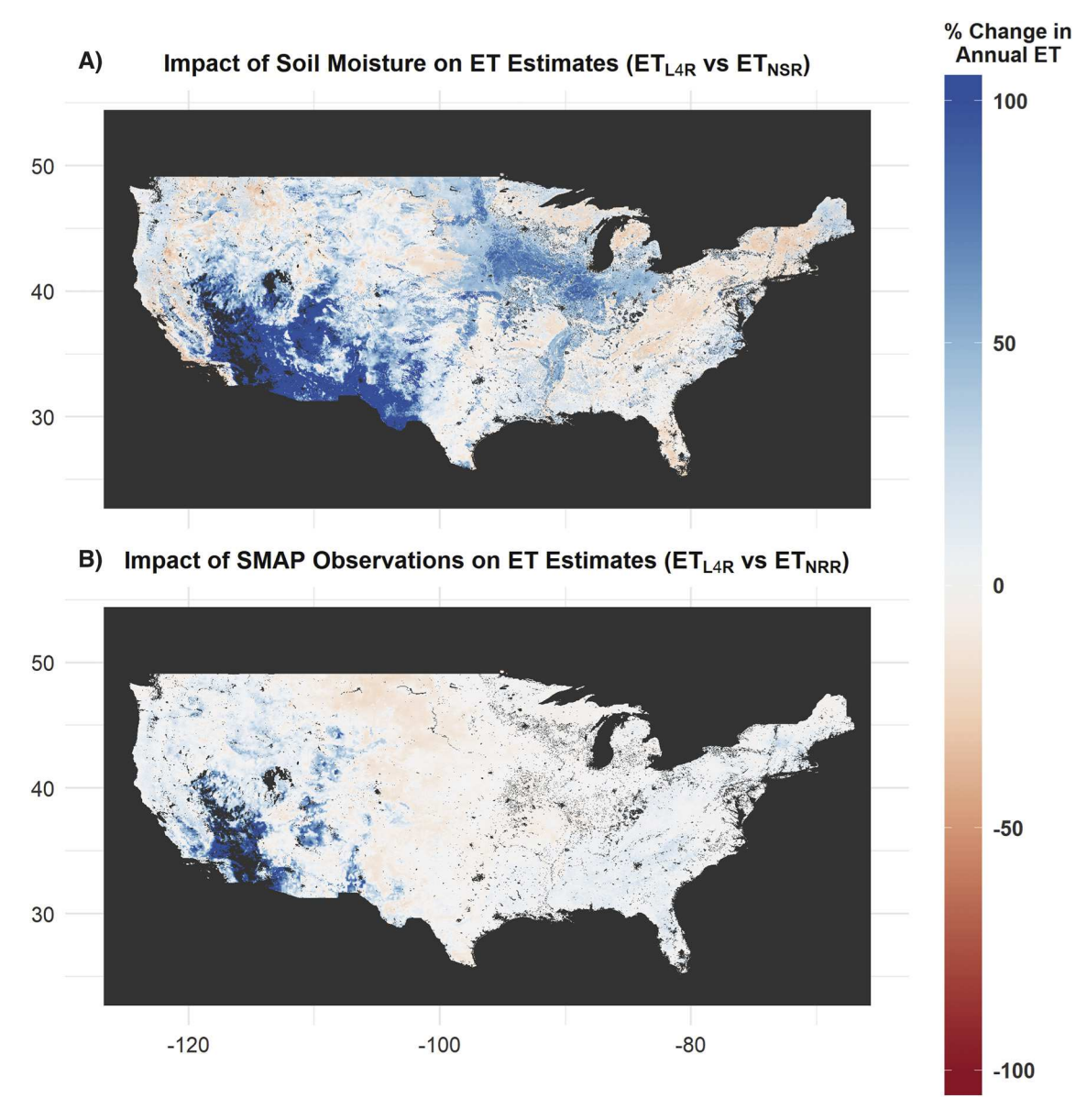


Fig. 6. Percent change in mean annual ET from ET_{L4R} compared to ET_{NSR} (A) and ET_{NRR} (B) for the 2015–2017 period; the difference maps are superimposed on a lat/lon grid and show the respective impacts of the added soil moisture control and SMAP observations on the model ET estimates. Blue (red) shades depict areas where ET_{L4R} predicts higher (lower) ET than the other models. Dark gray areas represent open water, barren land, and other areas excluded from the simulations and white reflect no change between model estimates. (For interpretation of the references to colour in this figure legend, the reader is referred to the web version of this article.)

updated model, transpiration is partially controlled by root zone soil moisture. Because the western CONUS is more arid than the east, the relatively low soil moisture conditions in the west impose further restrictions on ET_{L4R} (ET_{NRR}) transpiration relative to ET_{NSR} and ET_{MOD16G} (Fig. 8). As a result, the soil moisture-constrained models have a smaller component influence from transpiration than the models that are solely constrained by VPD and temperature. The estimated ratio of transpiration to ET from this study is also within the range of variability reported from previous studies (Stoy et al., 2019; Nelson et al., 2020) and follows similar spatial patterns of lower (higher) component transpiration influence in the western (eastern) CONUS (Zhang et al., 2019a). At the global scale, the baseline MOD16 method shows the transpiration to ET proportion to be approximately 24%, which is at the lower end of the fraction reported from other RS ET models (Miralles et al., 2016). While only provided for the CONUS domain, the transpiration to ET fractions from ET_{L4R} (ET_{NRR}) are more consistent with other reported model estimates (Miralles et al., 2016; Stoy et al., 2019).

The higher accuracy of the soil moisture-constrained models in arid regions may partially reflect greater SMAP soil moisture accuracy in areas with lower vegetation density. The L-band derived SMAP products are most sensitive to soil moisture where the overlying vegetation water content is less than $\sim 5 \text{ kg m}^{-2}$ (Entekhabi et al., 2010). The western CONUS is dominated by GRA, OSH and CSH, which tend to have less vegetation cover and associated greater L-band soil moisture sensitivity. In contrast, the eastern CONUS represents a more humid climate with greater vegetation density (e.g. forests), where the SMAP observations are expected to have less soil moisture sensitivity. The variable SMAP sensitivity pattern helps to explain why the largest SMAP impact on ET, indicated by the difference between ET_{NRR} and ET_{L4R}, occurs in the western CONUS (Fig. 6B). Here, the darker shades indicate where the model L4_SM soil moisture inputs propagate to larger differences in estimated annual ET relative to having no model soil moisture control (ET_{NSR}), or with a soil moisture control not directly informed by SMAP observations (ET_{NRR}).

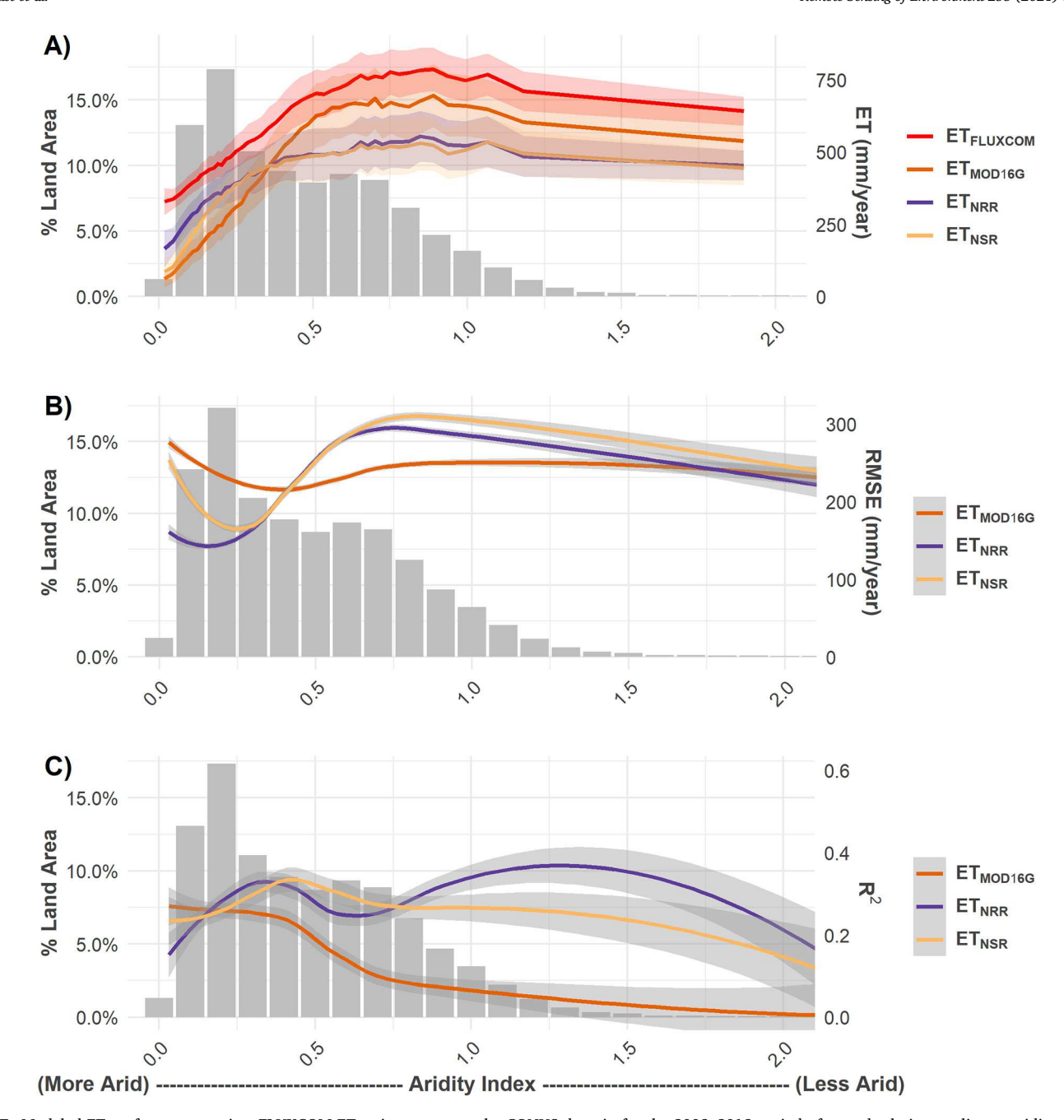


Fig. 7. Modeled ET performance against FLUXCOM ET estimates across the CONUS domain for the 2003–2013 period of record relative to climate aridity (AI; X-axis). The Y1 axis and gray bars show the distribution of CONUS land area falling within each AI category. The Y2 axis denotes estimated mean annual ET (A), RMSE (mm/year; B) and R^2 (C) calculated against FLUXCOM. AI values denote hyperarid (AI<0.03), arid (0.03 \leq AI<0.2), semi-arid (0.2 \leq AI<0.5), dry sub-humid (0.5 \leq AI<0.65), and humid (AI>0.65) conditions. Plotted lines are LOESS smoothed using an α parameter of 0.75, with shaded regions representing the standard error of the smoothing function.

Similar to the findings presented here, Purdy et al. (2018) found that the addition of SMAP Level 3 surface soil moisture (L3_SM) retrievals into the PT-JPL ET model were important in arid regions, but less relevant in humid climate regions. Here, there is little to no soil moisture influence on plant transpiration at humid sites, whereas transpiration at arid sites is heavily constrained by soil moisture (Fig. 9). In our study, the model improvements in arid regions are caused by increased ET relative to the baseline MOD16 product, which largely reflects an increase in soil evaporation. Partitioning of the underlying controls on estimated canopy stomatal conductance between temperature, VPD, and root zone soil moisture may reduce the model sensitivity to dynamic day-to-day fluctuations in VPD and temperature (Fig. 9); whereby, plant access to a more stable soil moisture resource helps to maintain ET

during periodic drought. Likewise, adding a surface soil moisture control to the model benefits from greater soil moisture memory in sustaining surface evaporation during drying cycles relative to the MOD16 baseline algorithm, which relies solely on an atmospheric moisture deficit derived control. Despite model improvements in arid regions, there is an abrupt increase in RMSE and an abrupt drop in $\rm R^2$ for ET_{NRR} in the most arid parts of the CONUS relative to FLUXCOM (Fig. 7B, C). In these arid regions, the coarse (9 km) resolution and small apparent wet bias in the L4_SM soil moisture record may contribute to the ET_{NRR} error (Reichle et al., 2017a).

An opposing negative bias between ET_{NRR} and ET_{NSR} is predominantly found in humid climate regions of the eastern CONUS that tend to be more energy than water limited (Nemani et al., 2003). In these areas,

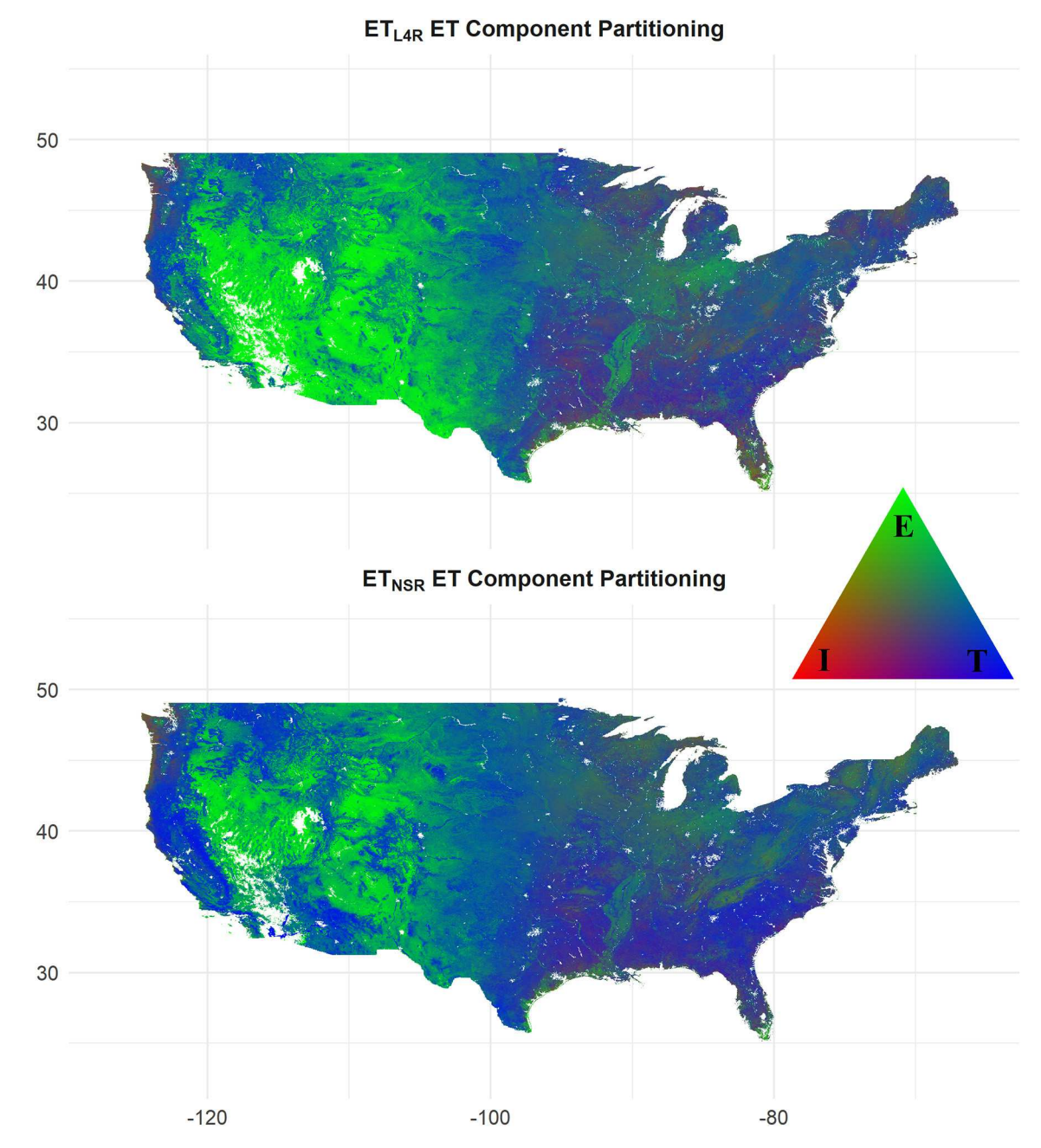


Fig. 8. ET component influence of plant transpiration (T, blue), soil evaporation (E, green), and canopy intercepted evaporation (I, red) for ET_{L4R} (top) and ET_{NSR} (bottom) from 2015 to 2017. Bright green, blue and red represent areas where ET is dominated by E, T, and I, respectively. Maps are depicted on a lat/lon grid. (For interpretation of the references to colour in this figure legend, the reader is referred to the web version of this article.)

there is generally sufficient soil water supply throughout the year for optimal transpiration, so that VPD and temperature are the dominant controls (Purdy et al., 2018; US-UMB in Fig. 9). As a result, the addition of a root zone soil moisture control has minimal effect, as seen by the similar ET_{NRR} and ET_{NSR} performance (Fig. 7A). In humid climates, ET_{MOD16G} has a slightly lower RMSE relative to FLUXCOM than both ET_{NRR} and ET_{NSR} (Fig. 7B). This is partially due to differences in FPAR/LAI gap filling methods between ET_{MOD16G} and ET_{NRR} (ET_{NSR}). In these regions, ET occurs at almost optimal rates, with less influence from environmental constraints (temperature, VPD, soil moisture) and more influence from the FPAR/LAI inputs on model performance. These regions also tend to have greater FPAR/LAI dropout and associated ET uncertainty due to clouds (Zhang et al., 2019a). FLUXCOM also tends to show slightly higher ET than other reported estimates in humid climate areas (Jung et al., 2019; Ma et al., 2020). This relative bias may

contribute to the observed FLUXCOM and $\rm ET_{NRR}$ (ET_{NSR}) differences. Additionally, the differences may reflect better $\rm ET_{NRR}$ representation of soil moisture as a control on ET. For example, $\rm ET_{NRR}$ estimates in southern Florida are lower relative to the other models (Figs. 5, 6A, S1), which reflects the coarse sandy soil texture and associated stronger model soil moisture control on ET in this region.

Spatially, the soil moisture-constrained models performed better in drier climate regions (AI<0.4) where ecosystems are more water limited. However, the importance of the soil moisture control also changes with time (Novick et al., 2016). For example, the ET_{NRR} and ET_{L4R} performance was most favorable between June and October at the arid US-Whs and US-Wkg towers (Fig. 3); whereas, both models overestimated ET during other months relative to the tower observations. The seasonally varying bias suggests the need for further model improvements in representing vegetation phenology, plant sensitivity to

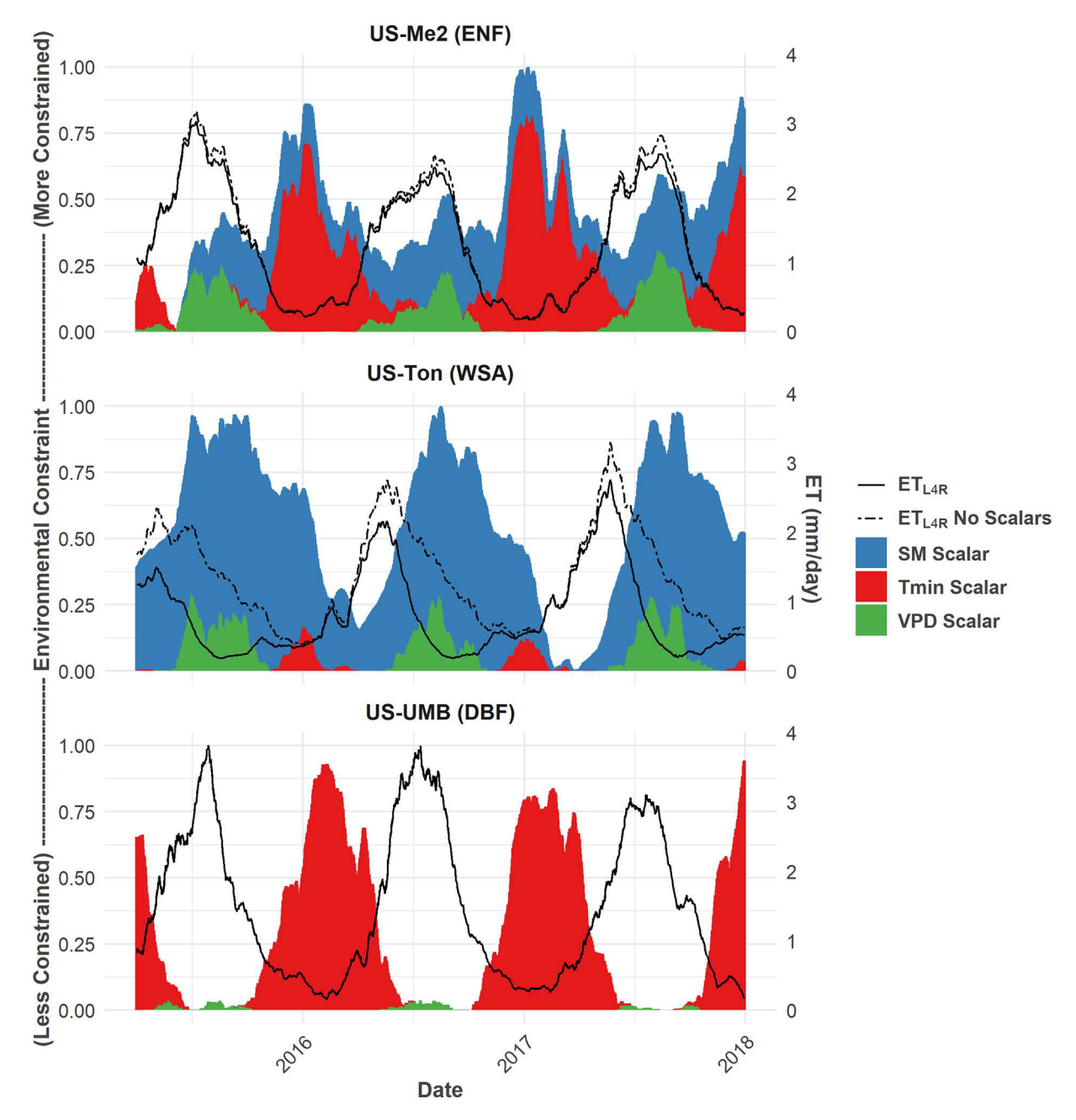


Fig. 9. Seasonal variations of estimated environmental restrictions on the model (ET_{L4R}) transpiration calculations for three flux tower sites representing major CONUS PFT classes. The relative influence from daily T_{min} , VPD, and root zone soil moisture (SM) by the respective environmental constraint (EC) scalars in Eqs. (9, 10, 18). The Y1 axis values represent EC and range between 0 (no constraint) and 1 (full constraint). The stacked colors represent the relative influence from each environmental factor on the model transpiration. The dotted line shows the maximum potential ET under minimal environmental constraints, while the solid line represents the estimated actual ET (Y2 axis). Plots were created by running the model with (solid line) and without (dotted line) all three EC scalars. The selected DBF, ENF and WSA sites are located in humid (AI = 0.73) and semi-arid (AI = 0.4, AI = 0.31) climate zones.

environmental stressors, and the seasonally varying importance of soil moisture and other controls. Improving understanding of the factors affecting ET seasonality should be a priority of future studies. As the effects of climate change progress, the traditional understanding of ET as being driven by VPD and soil moisture is expected to shift (Novick et al., 2016). For example, early spring greening driven by a warming climate may enhance ET, leading to summer soil moisture deficits (Lian et al., 2020). Failure to account for the influence of soil moisture on ET in such cases where soil water becomes insufficient to meet atmospheric demand could lead to notable model errors. Additionally, the projected changes in drought patterns will likely further complicate these relationships (Mo and Lettenmaier, 2015; Otkin et al., 2018). Better

understanding and representation of the abiotic and biotic impacts on ET is essential to improve RS ET models and properly quantify terrestrial water fluxes in the face of climate change.

6.3. Model uncertainties

Despite the improved model ET performance indicated from this study, the results still show significant remaining uncertainty. This uncertainty comes from three main sources, including: 1) the use of discrete model BPLUT parameterizations; 2) uncertainty in model inputs; and 3) the inability of the model to capture all physical processes affecting ET.

- 1. Discrete parameterizations. The underlying assumption of the MOD16 BPLUT based parameterizations is that the vegetation response to the various environmental factors affecting ET is largely consistent within individual biomes represented by a 12 PFT class global land cover map. However, variations in soil conditions, vegetation structure and age class, and other factors can lead to significant ET heterogeneity within a given biome. This variable response can be seen in the standard deviations of the model parameters (Tables S2, S3). All parameters show variability around the mean, reflecting inherent uncertainty in parameter values that can contribute to model ET error. Additionally, as plants near stress, complex and non-linear interactions of soil moisture and VPD can drive stomatal conductance (Novick et al., 2016), further contributing to uncertainty when using the simple linear efficiency functions and open/close parameters outlined in Eq. 8. This is evident in Table S2, where variability in the SM_{open} and SM_{close} parameters are large for CSH, OSH and WSA, reflecting the uncertainty in the parameter values within the relatively coarse PFT classes. The potential use of more spatially variable parameterizations incorporating data-driven machine learning or hybrid modeling approaches may lead to further model improvements over BPLUT based methods (Madani et al., 2017; Jung et al., 2019; Reichstein et al., 2019; Tramontana et al., 2016) and should be pursued as a priority research topic.
- 2. Model input uncertainty. All inputs to the MOD16 algorithm have uncertainty, which can contribute to model ET error. For example, the SMAP L4_SM product has a targeted mean accuracy of 0.04 m³ m⁻³ for surface and root zone soil moisture (Reichle et al., 2019). Additional uncertainty is contributed from the MODIS LAI/FPAR and land cover products used as model inputs due to algorithm assumptions, atmospheric contamination, sensor footprint and calibration uncertainty, and other factors (Miura et al., 2000; Xu et al., 2018). Additionally, the models presented here rely on modeled Gridmet meteorology. While Gridmet provides approximately 10fold improved spatial resolution over that of the global GEOS FP-IT meteorology used in the baseline MOD16 product, the 4 km Gridmet resolution may still not adequately resolve microclimate spatial heterogeneity (Walton and Hall, 2018; Behnke et al., 2016; Zhao et al., 2005), which may contribute to model ET uncertainty. Additionally, soil moisture can vary significantly within the 9 km SMAP scale. Although the REW conversion in Eq. 17 compresses relative variability by effectively normalizing soil moisture across a pixel, formal downscaling is necessary to capture the heterogeneity at the 500 m scale with more fidelity. Future studies should explore implementing downscaled soil moisture into ET modeling frameworks to further improve ET estimates (Chaney et al., 2016; Colliander et al., 2017; Fang et al., 2020).
- 3. Missing processes. Because ET is a complex process, simplifying assumptions must be made to facilitate regional to global scale model predictions. For example, wind speed, soil type, and precipitation can significantly influence ET, but are missing from our model (Purdy et al., 2018; McVicar et al., 2012; He et al., 2019b). Rooting depth is also a key variable in estimating ET, as it determines where in the soil profile a plant has access to water (Guswa, 2010). This may be a cause of uncertainty in our modeling framework, as we assume that root zone (0–1 m) soil moisture drives transpiration even though rooting depths can exceed 3 m (Yang et al., 2016). Finally, model parameters representing physical processes such as the aerodynamic resistance to soil evaporation (*rbl*_{min} and *rbl*_{max}) are difficult to measure in situ, contributing to greater uncertainty in parameter boundaries (Mu et al., 2011).

7. Conclusion

This study improves estimates of ET in the CONUS domain by recalibrating the model, introducing high-resolution Gridmet meteorology,

and adding a SMAP informed soil moisture control to the MOD16 algorithm. We adapted the MOD16 framework to include a root zone soil moisture control on plant transpiration and a surface soil moisture control on soil evaporation. The model was calibrated at 69 AmeriFlux tower sites representing 10 diverse PFTs across the entire CONUS domain. The model was validated using a holdout set of flux tower data and the FLUXCOM product to assess our objectives. We found that (i) the added soil moisture controls, Gridmet meteorology and regional calibration improved model performance over the MOD16 global baseline relative to ET observations from regional flux towers; (ii) these results are more pronounced in dry land areas of the western CONUS and when ecosystems are water limited. The soil moisture constrained model shows the greatest improvements in arid and semi-arid regions (AI<0.4), which represent approximately 40% of the global land area (Smith et al., 2019). The resulting model provides new capacity for monitoring the effects of drought and climate change on the water cycle, while providing a new framework for investigating both soil and atmosphere controls on ET.

CRediT authorship contribution statement

Colin Brust: Conceptualization, Methodology, Software, Writing - original draft, Writing - review & editing.

John S. Kimball: Conceptualization, Methodology, Funding acquisition, Writing - review & editing.

Marco P. Maneta: Methodology, Funding acquisition, Writing - review & editing.

Kelsey Jencso: Conceptualization, Methodology, Writing - review & editing.

Mingzhu He: Software, Writing - review & editing. Rolf H. Reichle: Writing - review & editing.

Declaration of Competing Interest

The authors declare that they have no known competing financial interests or personal relationships that could have appeared to influence the work reported in this paper.

Acknowledgements

This study was conducted at the University of Montana with funding provided by NASA (NNH17ZHA002C, NNX14AI50G, 80NSSC18M0025M) and the USDA NIFA (National Institute of Food and Agriculture) program (658 2016-67026-25067). R. Reichle was supported by the SMAP Science Team. This work used eddy covariance data acquired and shared by the FLUXNET community, including the AmeriFlux network. FLUXCOM data are available through the Max Planck Institute for Biogeochemistry at http://fluxcom.org. Thanks to Dr. Tim McVicar and three other anonymous reviewers whose comments and feedback greatly improved this manuscript.

Appendix A. Supplementary data

Supplementary data to this article can be found online at https://doi.org/10.1016/j.rse.2020.112277.

References

Abatzoglou, John T., 2013. Development of gridded surface meteorological data for ecological applications and modelling. Int. J. Climatol. 33 (1), 121–131. https://doi. org/10.1002/joc.3413.

Allen, R.G., Tasumi, M., Morse, A., Trezza, R., Wright, J.L., Bastiaanssen, W., Kramber, W., Lorite, I.J., Robinson, C.W., 2007. Satellite-based energy balance for mapping evapotranspiration with internalized calibration (METRIC)— applications. J. Irrig. Drain. Eng. 133 (4), 395–406. https://doi.org/10.1061/(ASCE)0733-9437 (2007)133.

Arriga, Nicola, Rannik, Üllar, Aubinet, Marc, Carrara, Arnaud, Vesala, Timo, Papale, Dario, 2017. Experimental validation of footprint models for Eddy

- covariance CO2 flux measurements above grassland by means of natural and artificial tracers. Agric. For. Meteorol. 242 (May), 75–84. https://doi.org/10.1016/j.agrfc/mpt. 2017.04.06
- Baldocchi, Dennis D., 2003. Assessing the Eddy covariance technique for evaluating carbon dioxide exchange rates of ecosystems: past, present and future. Glob. Chang. Biol. 9 (October 2002), 479–492. https://doi.org/10.1016/0376-6357(93)90090-E.
- Baldocchi, Dennis, Falge, Eva, Lianhong, Gu, Olson, Richard, Hollinger, David, Running, Steve, Anthoni, Peter, et al., 2001. FLUXNET: a new tool to study the temporal and spatial variability of ecosystem-scale carbon dioxide, water vapor, and energy flux densities. Bull. Am. Meteorol. Soc. 82 (11), 2415–2434. https://doi.org/ 10.1175/1520-0477(2001)082
- Barcza, Z., Kern, A., Haszpra, L., Kljun, N., 2009. Spatial representativeness of tall tower Eddy covariance measurements using remote sensing and footprint analysis. Agric. For. Meteorol. 149 (5), 795–807. https://doi.org/10.1016/j.agrformet.2008.10.021.
- Behnke, R., Vavrus, S., Allstadt, A., Albright, T., Thogmartin, W.E., Radeloff, V.C., 2016. Evaluation of downscaled, gridded climate data for the conterminous United States. Ecol. Appl. 26 (5), 1338–1351. https://doi.org/10.1002/15-1061.
- Brodzik, Mary J., Billingsley, Brendan, Haran, Terry, Raup, Bruce, Savoie, Matthew H., 2014. Correction: EASE-Grid 2.0: Incremental but significant improvements for earth-gridded data sets (ISPRS International Journal of Geo-Information (2012) 1 (32–45)). ISPRS Int. J. Geo Inf. 3 (3), 1154–1156. https://doi.org/10.3390/ijgi3031154.
- Chaney, N.W., Metcalfe, P., Wood, E.F., 2016. HydroBlocks: a field-scale resolving land surface model for application over continental extents. Hydrol. Process. 30 (20), 3543–3559. https://doi.org/10.1002/hyp.10891.
- Colliander, Andreas, Fisher, Joshua B., Halverson, Gregory, Merlin, Olivier, Misra, Sidhartha, Bindlish, Rajat, Jacks, Thomas J., et al., 2017. Spatial downscaling of SMAP soil moisture using MODIS Land surface temperature and NDVI during SMAPVEX15. IEEE Geosci. Remote Sens. Lett. 14 (11), 2107–2111. https://doi.org/ 10.1109/LGRS.2017.2753203.
- Entekhabi, Dara, Njoku, Eni G., Neill, Peggy E.O., Kellogg, Kent H., Crow, Wade T., Edelstein, Wendy N., Entin, Jared K., et al., 2010. The soil moisture active passive (SMAP) mission. Proc. IEEE 98 (5).
- Fang, Li, Zhan, Xiwu, Yin, Jifu, Liu, Jicheng, Schull, Mitchell, Walker, Jeffrey P., Wen, Jun, et al., 2020. An intercomparison study of algorithms for downscaling SMAP radiometer soil moisture retrievals. J. Hydrometeorol. 21, 1761–1775. https://doi.org/10.1175/JHM-D-19-0034.1.
- Fisher, Joshua B., Tu, Kevin P., Baldocchi, Dennis D., 2008. Global estimates of the landatmosphere water flux based on monthly AVHRR and ISLSCP-II data, validated at 16 FLUXNET sites. Remote Sens. Environ. 112, 901–919. https://doi.org/10.1016/j. rse.2007.06.025.
- Fisher, Joshua B., Melton, Forrest, Middleton, Elizabeth, Hain, Christopher, Anderson, Martha, Allen, Richard, McCabe, Matthew F., et al., 2017. The future of evapotranspiration: global requirements for ecosystem functioning, carbon and climate feedbacks, agricultural management, and water resources. Water Resour. Res. 53 (4), 2618–2626. https://doi.org/10.1002/2016WR020175.
- Foken, T., Wimmer, F., Mauder, M., Thomas, C., Liebethal, C., 2006. Some aspects of the energy balance closure problem. Atmos. Chem. Phys. 6 (12), 4395–4402. https://doi.org/10.5194/acp-6-4395-2006
- Friedl, M.A., McIver, D.K., Hodges, J.C.F., Zhang, X.Y., Muchoney, D., Strahler, A.H., Woodcock, C.E., et al., 2002. Global land cover mapping from MODIS: algorithms and early results. Remote Sens. Environ. 83 (1–2), 287–302. https://doi.org/ 10.1016/S0034-4257(02)00078-0
- Gardner, W.R., Ehlig, C.F., 1963. The influence of soil water on transpiration by plants. J. Geophys. Res. 68 (20), 5719–5724. https://doi.org/10.1029/jz068i020p05719.
- Gorelick, Noel, Hancher, Matt, Dixon, Mike, Ilyushchenko, Simon, Thau, David, Moore, Rebecca, 2017. Google earth engine: planetary-scale geospatial analysis for everyone. Remote Sens. Environ. 202, 18–27. https://doi.org/10.1016/j. rse.2017.06.031.
- Guswa, A.J., 2010. Effect of plant uptake strategy on the water-optimal root depth. Water Resour. Res. 46 (9), 1–5. https://doi.org/10.1029/2010WR009122.
- He, Mingzhu, Kimball, John S., Running, Steven, Ballantyne, Ashley, Guan, Kaiyu, Huemmrich, Fred, 2016. Satellite detection of soil moisture related water stress impacts on ecosystem productivity using the MODIS-based photochemical reflectance index. Remote Sens. Environ. 186, 173–183. https://doi.org/10.1016/j.rss.2016.08.019
- He, Mingzhu, Kimball, John S., Yi, Yonghong, Running, Steve, Guan, Kaiyu, Jencso, Kelsey, Maxwell, Bruce, Maneta, Marco, 2019a. Impacts of the 2017 flash drought in the US Northern Plains informed by satellite-based evapotranspiration and solar-induced fluorescene. Environ. Res. Lett. https://doi.org/10.1088/1748-9326/ab22c3
- He, Mingzhu, Kimball, John S., Yi, Yonghong, Running, Steven W., Guan, Kaiyu, Moreno, Alvaro, Wu, Xiaocui, Maneta, Marco, 2019b. Satellite data-driven modeling of field scale evapotranspiration in croplands using the MOD16 algorithm framework. Remote Sens. Environ. 230 (December 2018), 111201. https://doi.org/10.1016/j.rse.2019.05.020.
- IPCC, 2014. Climate Change 2014: Synthesis Report; Contribution of Working Groups I, II, and III to the Fifth Assessment Report of the Intergovernmental Panel on Climate Change. IPCC, Geneva, Switzerland. https://doi.org/10.1046/j.1365-2559.2002.1340a.x.
- Jones, Lucas A., Kimball, John S., Reichle, Rolf H., Madani, Nima, Glassy, Joe, Ardizzone, Joe V., Colliander, Andreas, et al., 2017. The SMAP level 4 carbon product for monitoring ecosystem land-atmosphere CO2 exchange. IEEE Trans. Geosci. Remote Sens. 55 (11), 6517–6532. https://doi.org/10.1109/TGRS.2017.2729343.

- Jung, Martin, Reichstein, Markus, Margolis, Hank A., Cescatti, Alessandro, Richardson, Andrew D., Arain, M. Altaf, Arneth, Almut, et al., 2011. Global patterns of land-atmosphere fluxes of carbon dioxide, latent heat, and sensible heat derived from Eddy covariance, satellite, and meteorological observations. J. Geophys. Res. Biogeosci. 116 (3), 1–16. https://doi.org/10.1029/2010JG001566.
- Jung, Martin, Koirala, Sujan, Weber, Ulrich, Ichii, Kazuhito, Gans, Fabian, Camps-Valls, Gustau, Papale, Dario, Schwalm, Christopher, Tramontana, Gianluca, Reichstein, Markus, 2019. The FLUXCOM ensemble of global land-atmosphere energy fluxes. Sci. Data 6 (1), 74. https://doi.org/10.1038/s41597-019-0076-8.
- Khan, Muhammad Sarfraz, Liaqat, Umar Waqas, Baik, Jongjin, Choi, Minha, 2018. Standalone uncertainty characterization of GLEAM, GLDAS and MOD16 evapotranspiration products using an extended triple collocation approach. Agric. For. Meteorol. 252 (October 2017), 256–268. https://doi.org/10.1016/j.agrformet.2018.01.022.
- Koster, Randal D., Suarez, Max J., Ducharne, Agnès, Stieglitz, Marc, Kumar, Praveen, 2000. A catchment-based approach to modeling land surface processes in a general circulation model: 1. Model structure. J. Geophys. Res.-Atmos. 105 (D20), 24809–24822. https://doi.org/10.1029/2000jd900328.
- Lian, Xu, Piao, Shilong, Li, Laurent Z.X., Li, Yue, Huntingford, Chris, Ciais, Philippe, Cescatti, Alessandro, et al., 2020. Summer soil drying exacerbated by earlier spring greening of northern vegetation. Sci. Adv. 6 (1), 1–12. https://doi.org/10.1126/ sciadv.aax0255.
- Lu, Nan, Chen, Shiping, Wilske, Burkhard, Sun, Ge, Chen, Jiquan, 2011. Evapotranspiration and soil water relationships in a range of disturbed and undisturbed ecosystems in the semi-arid Inner Mongolia, China. J. Plant Ecol. 4 (1–2), 49–60. https://doi.org/10.1093/jpe/rtq035.
- Lucchesi, R., 2015. "File Specification for GEOS-5 FP-IT (Forward Processing for Instrument Teams)." Greenbelt, MD. https://gmao.gsfc.nasa.gov/pubs/docs/Lucche si865.pdf.
- Ma, N., Szilagyi, Jozsef, Jozsa, Janos, 2020. Benchmarking large-scale evapotranspiration estimates: a perspective from a calibration-free complementary relationship approach and FLUXCOM. J. Hydrol. 590 https://doi.org/10.1016/j. ihydrol.2020.125221.
- Madani, N., Kimball, J.S., Running, S.W., 2017. Improving global gross primary productivity estimates by computing optimum light use efficiencies using flux tower data. J. Geophys. Res. Biogeosci. 122 (11), 2939–2951. https://doi.org/10.1002/ 2017/IG004142
- Maneta, M.P., Silverman, N.L., 2013. A spatially distributed model to simulate water, energy, and vegetation dynamics using information from regional climate models. Earth Interact. 17 (11) https://doi.org/10.1175/2012E1000472.1.
- Martens, B., Miralles, Diego G., Lievens, Hans, van der Schalie, Robin, de Jeu, Richard A. M., Fernandez-Prieto, Diego, Beck, Hylke E., et al., 2017. GLEAM v3: Satellite-based land evaporation and root-zone soil moisture. Geosci. Model Dev. 10, 1903–1925. https://doi.org/10.5194/emd-10-1903-2017.
- McCabe, M.F., Ershadi, A., Jimenez, C., Miralles, D.G., Michel, D., Wood, E.F., 2016. The GEWEX LandFlux project: evaluation of model evaporation using tower-based and globally gridded forcing data. Geosci. Model Dev. 9 (1), 283–305. https://doi.org/ 10.5194/pmd.9-283-2016
- McVicar, Tim R., Roderick, Michael L., Donohue, Randall J., Li, Ling Tao, Van Niel, Thomas G., Thomas, Axel, Grieser, Jürgen, et al., 2012. Global review and synthesis of trends in observed terrestrial near-surface wind speeds: implications for evaporation. J. Hydrol. 416–417, 182–205. https://doi.org/10.1016/j.ibydrol.2011.10.024.
- Michel, D., Jiménez, C., Miralles, D.G., Jung, M., Hirschi, M., Ershadi, A., Martens, B., et al., 2016. The WACMOS-ET project part 1: tower-scale evaluation of four remote-sensing-based evapotranspiration algorithms. Hydrol. Earth Syst. Sci. 20 (2), 803–822. https://doi.org/10.5194/hess-20-803-2016.
- Miralles, D.G., Jimenez, C., Jung, M., Michel, D., Ershadi, A., McCabe, M.F., Hirschi, M., et al., 2016. The WACMOS-ET project part 2: evaluation of global terrestrial evaporation data sets. Hydrol. Earth Syst. Sci. 20 (2), 823–842. https://doi.org/10.5194/hess-20-823-2016.
- Miura, T., Huerte, A.R., Yoshioka, H., 2000. Evaluation of sensor calibration uncertainties on vegetation indices for MODIS. IEEE Trans. Geosci. Remote Sens. 38 (3), 1399–1409.
- Mo, Kingtse C., Lettenmaier, Dennis P., 2015. Heat wave flash droughts in decline. Geophys. Res. Lett. 42 (8), 2823–2829. https://doi.org/10.1002/2015GL064018.
- Moreira, Adriana Aparecida, Ruhoff, Anderson Luis, Roberti, Débora Regina, de Arruda Souza, Vanessa, da Rocha, Humberto Ribeiro, de Paiva, Rodrigo Cauduro Dias, 2019. Assessment of terrestrial water balance using remote sensing data in South America. J. Hydrol. 575 (December 2018), 131–147. https://doi.org/10.1016/j. ihydrol.2019.05.021.
- Mu, Qiaozhen, Heinsch, Faith Ann, Zhao, Maosheng, Running, Steven W., 2007. Development of a global evapotranspiration algorithm based on MODIS and global meteorology data. Remote Sens. Environ. 111 (4), 519–536. https://doi.org/ 10.1016/j.rse.2007.04.015.
- Mu, Qiaozhen, Zhao, Maosheng, Running, Steven W., 2011. Improvements to a MODIS global terrestrial evapotranspiration algorithm. Remote Sens. Environ. 115 (8), 1781–1800. https://doi.org/10.1016/j.rse.2011.02.019.
- Myneni, R.B., Hoffman, S., Knyazikhin, Y., Privette, J.L., Glassy, J., Tian, Y., Wang, Y., et al., 2002. Global products of vegetation leaf area and fraction absorbed PAR from year one of MODIS data. Remote Sens. Environ. 83 (1–2), 214–231. https://doi.org/10.1016/S0034-4257(02)00074-3.
- Nelson, Jacob A., Pérez-Priego, O., Zhou, S., et al., 2020. Ecosystem transpiration and evaporation: insights from three water flux partitioning methods across FLUXNET sites. Glob. Chang. Biol. 00, 1–15. https://doi.org/10.1111/gcb.15314.

- Nemani, R.R., Keeling, Charles D., Hashimoto, Hirofumi, Jolly, William M., Piper, Stephen C., Tucker, Compton J., Myneni, Ranga B., Running, Steven W., 2003. Climate-driven increases in global terrestrial net primary production from 1982 to 1999. Science (80-.) 300, 1560–1563. https://doi.org/10.1126/science.1082750.
- Novák, V., Hurtalová, T., Matejka, F., 2005. Predicting the effects of soil water content and soil water potential on transpiration of maize. Agric. Water Manag. 76 (3), 211–223. https://doi.org/10.1016/j.agwat.2005.01.009.
- Novick, Kimberly A., Ficklin, Darren L., Stoy, Paul C., Williams, Christopher A., Bohrer, Gil, Christopher Oishi, A., Papuga, Shirley A., et al., 2016. The increasing importance of atmospheric demand for ecosystem water and carbon fluxes. Nat. Clim. Chang. 6 (11), 1023–1027. https://doi.org/10.1038/nclimate3114.
- Oki, Taikan, Kanae, Shinjiro, 2006. Global hydrological cycles and world water. Science 313 (August), 1068–1073. https://doi.org/10.1126/science.1128845.
- Otkin, Jason A., Svoboda, Mark, Hunt, Eric D., Ford, Trent W., Anderson, Martha C., Hain, Christopher, Basara, Jeffrey B., 2018. Flash droughts: a review and assessment of the challenges imposed by rapid-onset droughts in the United States. Bull. Am. Meteorol. Soc. 99 (5), 911–919. https://doi.org/10.1175/BAMS-D-17-0149.1.
- Pastorello, G., Papale, D., Chu, H., Trotta, C., Agarwal, D., Canfora, E., Baldocchi, D., Torn, M., 2017. A new data set to keep a sharper eye on land-air exchanges. Eos (August). https://doi.org/10.1029/2017eo071597.
- Purdy, Adam J., Fisher, Joshua B., Goulden, Michael L., Colliander, Andreas, Halverson, Gregory, Tu, Kevin, Famiglietti, James S., 2018. SMAP soil moisture improves global evapotranspiration. Remote Sens. Environ. 219 (December 2017), 1–14. https://doi.org/10.1016/j.rse.2018.09.023.
- Reichle, Rolf H., De Lannoy, Gabrielle J.M., Liu, Qing, Koster, Randal D., Kimball, John S., Crow, Wade T., Ardizzone, Joseph V., et al., 2017a. Global assessment of the SMAP Level-4 surface and root-zone soil moisture product using assimilation diagnostics. J. Hydrometeorol. 18 (12), 3217–3237. https://doi.org/10.1175/JHM-D-17-0130.1
- Reichle, Rolf H., Seyfried, Mark, Smith, Edmond B., Livingston, Stan, De Lannoy, Gabrielle J.M., Pellarin, Thierry, Jensen, Karsten H., et al., 2017b. Assessment of the SMAP Level-4 surface and root-zone soil moisture product using in situ measurements. J. Hydrometeorol. 18 (10), 2621–2645. https://doi.org/ 10.1175/jhm-d-17-0063.1.
- Reichle, Rolf H., De Lannoy, Gabrielle J.M., Koster, Randal D., Crow, Wade T., Kimball, John S., Liu, Q., 2018. SMAP L4 Global 3-Hourly 9 Km EASE-Grid Surface and Root Zone Soil Moisture Geophysical Data, Version 4. NASA National Snow and Ice Data Center DAAC. https://doi.org/10.5067/kpjinn2gi1dgr.
- Reichle, Rolf H., Liu, Qing, Koster, Randal D., Crow, Wade T., De Lannoy, Gabrielle J.M., Kimball, John S., Ardizzone, Joseph V., et al., 2019. Version 4 of the SMAP Level-4 soil moisture algorithm and data product. J. Adv. Model. Earth Syst. 3106–3130. https://doi.org/10.1029/2019MS001729.
- Reichstein, M., Camps-Valls, Gustau, Stevens, Bjorn, Jung, Martin, Denzler, Joachim, Carvalhais, Nuno, Prabhat, 2019. Deep learning and process understanding for data-driven Earth system science. Nature 566, 195–204. https://doi.org/10.1038/s41586-019-0912-1.
- Rienecker, M.M., Suarez, M.J., Todling, R., Bacmeister, J., Takacs, L., Liu, H.C., Gu, W., et al., 2008. "The GEOS-5 Data Assimilation System -Documentation of Versions 5.0.1. 5.1.0." Washington, DC.
- Ruhoff, A.L., Paz, A.R., Aragao, L.E.O.C., Mu, Q., Malhi, Y., Collischonn, W., Rocha, H.R., Running, S.W., 2013. Assessment of the MODIS global evapotranspiration algorithm using Eddy covariance measurements and hydrological modelling in the Rio Grande basin. Hydrol. Sci. J. 58 (8), 1658–1676. https://doi.org/10.1080/026565.2013.937578
- Schaaf, C., Wang, Z., 2015. MCD43A3 MODIS/Terra+Aqua BRDF/Albedo daily L3 global - 500m V006. In: NASA EOSDIS Land Processes DAAC. https://doi.org/10.5067/ MODIS/MCD43A3.006.
- Short Gianotti, Daniel J., Rigden, Angela J., Salvucci, Guido D., Entekhabi, Dara, 2019. Satellite and station observations demonstrate water availability's effect on

- continental-scale evaporative and photosynthetic land surface dynamics. Water Resour. Res. 55 (1), 540-554. https://doi.org/10.1029/2018WR023726.
- Smith, W.K., Dannenberg, Matthew P., Yan, Dong, Herrmann, Stefanie, Barnes, Mallory L., Barron-Gafford, Greg A., Biederman, Joel A., et al., 2019. Remote sensing of dryland ecosystem structure and function: Progress, challenges, and opportunities. Remote Sens. Environ. 233, 111401 https://doi.org/10.1016/j.rse.2019.111401.
- Stoy, P.C., El-Madany, Tarek, Fisher, Joshua B., Gentine, Pierre, Gerken, Tobias, Good, Stephen P., et al., 2019. Reviews and syntheses: Turning the challenges of partitioning ecosystem evaporation and transpiration into opportunities. Biogeosci. Discuss. 1–47. https://doi.org/10.5194/bg-2019-85.
- Tramontana, G., Martin Jung, Christopher R., Schwalm, Kazuhito Ichii, Camps-Valls, Gustau, Raduly, Botond, Reichstein, Markus, et al., 2016. Predicting carbon dioxide and energy fluxes across global FLUXNET sites with regression algorithms. Biogeosciences 13, 4291–4313 (2016).
- United Nations Educational, Scientific and Cultural Organization (UNESCO), 1979. Map of the World Distribution of Arid Regions: Map at Scale 1:25000000 with Explanator Note. UNESCO, Paris.
- Walton, Daniel, Hall, Alex, 2018. An assessment of high-resolution gridded temperature datasets over California. J. Clim. 31 (10), 3789–3810. https://doi.org/10.1175/
- Wu, Yuanzhi, Huang, Mingbin, Gallichand, Jacques, 2011. Transpirational response to water availability for winter wheat as affected by soil textures. Agric. Water Manag. 98 (4), 569–576. https://doi.org/10.1016/j.agwat.2010.10.015.
- Wurster, Patrick, Maneta, Marco, Begueria, Santiago, Cobourn, Kelly, Maxwell, Bruce, Silverman, Nick, Ewing, Stephanie, et al., 2020. Characterizing the impact of climatic and price anomalies on agrosystems in the Northwest United States. Agric. For. Meteorol. 280 (November 2018) https://doi.org/10.1016/j.agrformet 2019 107778
- Xu, Baodong, Park, Taejin, Yan, Kai, Chen, Chi, Zeng, Yelu, Song, Wanjuan, Yin, Gaofei, et al., 2018. Analysis of global LAI/FPAR products from VIIRS and MODIS sensors for spatio-temporal consistency and uncertainty from 2012–2016. Forests 9 (2), 1–21. https://doi.org/10.3390/f9020073.
- Yang, Y., Donohue, R.J., McVicar, T.R., 2016. Global estimation of effective plant rooting depth: implications for hydrological modeling. Water Resour. Res. 52 (10), 8260–8276. https://doi.org/10.1002/2016WR019392.
- Zhang, Ke, Kimball, John S., Running, Steven W., 2016a. A review of remote sensing based actual evapotranspiration estimation. Wiley Interdiscip. Rev. Water 3 (6), 834–853. https://doi.org/10.1002/wat2.1168.
- Zhang, Yongqiang, Peña-Arancibia, Jorge L., McVicar, Tim R., Chiew, Francis H.S., Vaze, Jai, Liu, Changming, Lu, Xingjie, et al., 2016b. Multi-decadal trends in global terrestrial evapotranspiration and its components. Sci. Rep. 6 (January), 1–12. https://doi.org/10.1038/srep19124.
- Zhang, Yongqiang, Kong, Dongdong, Gan, Rong, Chiew, Francis H.S., Mcvicar, Tim R.,
 Zhang, Qiang, Yang, Yuting, 2019a. Coupled Estimation of 500 m and 8-Day
 Resolution Global Evapotranspiration and Gross Primary Production in 2002–2017.
 Remote Sens. Environ. 222, 165–182. May 2018. (doi:S003442571830590X).
- Zhang, Kun, Zhu, Gaofeng, Ma, Jinzhu, Yang, Yuting, Shang, Shasha, Gu, Chunjie, 2019b. Parameter analysis and estimates for the MODIS evapotranspiration algorithm and multiscale verification. Water Resour. Res. 55 (3), 2211–2231. https://doi.org/10.1029/2018WR023485
- Zhang, Baoqing, Xia, Youlong, Long, Biao, Hobbins, Mike, Zhao, Xining, Hain, Christopher, Li, Yaohui, Anderson, Martha C., 2020. Evaluation and comparison of multiple evapotranspiration data models over the contiguous United States: implications for the next phase of NLDAS (NLDAS-testbed) development. Agric. For. Meteorol. 280 (March 2019), 107810. https://doi.org/10.1016/j.agrformet 2019 107810
- Zhao, Maosheng, Heinsch, Faith Ann, Nemani, Ramakrishna R., Running, Steven W., 2005. Improvements of the MODIS terrestrial gross and net primary production global data set. Remote Sens. Environ. 95 (2), 164–176. https://doi.org/10.1016/j. rss. 2004.12.011